O-Alkyl hydroxamates display potent and selective antileishmanial activity

Victoriano Corpas-López,^{#b} Mavys Tabraue-Chavez,^{#a} Yudibeth Sixto- López,^e Sonia Panadero-Fajardo,^a Fernando Alves de Lima Franco,^{bβ} José F. Domínguez-Seglar,^a Francisco Morillas-Márquez,^b Francisco Franco-Montalbán,^a Mónica Díaz-Gavilán,^a José Correa-Basurto,^e Julián López-Viota,^{cα} Margarita López-Viota,^c José Pérez del Palacio,^d Mercedes de la Cruz,^d Nuria de Pedro,^d Joaquina Martín-Sánchez,^b José A. Gómez-Vidal*^a

- (a) Departamento de Química Farmacéutica y Orgánica, Facultad de Farmacia, Universidad de Granada, Campus de Cartuja, 18071 Granada, Spain
- (b) Departamento de Parasitología, Facultad de Farmacia, Universidad de Granada, Campus de Cartuja, 18071 Granada, Spain
- (c) Departamento de Farmacia y Tecnología Farmacéutica, Facultad de Farmacia, Universidad de Granada, Campus de Cartuja, 18071 Granada, Spain
- (d) Fundación MEDINA, Parque Tecnológico de la Salud, Granada, Spain
- (e) Laboratorio de Diseño y Desarrollo de Nuevos Fármacos y Productos Biotecnológicos, Sección de Estudios de Posgrado e Investigación, Escuela Superior de Medicina, Instituto Politécnico Nacional, Plan de San Luis y Díaz Mirón, 11340, México City, México
- (α) Present address at Vircell, Parque Tecnológico de la Salud, Avicena 8, 18016 Granada, Spain
- (β) Present address at Faculdade Israelita de Ciências da Saúde Albert Einstein FICSAE, Nursing Course, São Paulo, SP, Postal Code 05521-200, Brazil

Abstract

Leishmania (L.) infantum causes visceral, cutaneous and mucosal leishmaniasis in humans and canine leishmaniasis in dogs. Herein, we describe that *O*-alkyl hydroxamate derivatives displayed potent and selective *in vitro* activity against the amastigote stage of *L. infantum* while no activity was observed against promastigotes. Compound **5** showed potent *in vivo* activity against *L. infantum*. Moreover, the combination of compound **5** supported on gold nanoparticles and meglumine antimoniate was also effective *in vivo* and improved the activity

of these compounds compared to that of the individual treatment. Docking studies showed that compound **5** did not reach highly conserved pocket C and established interactions with the semiconserved residues V44, A45, R242, and E243 in pocket A of LiSIR2rp1. The surface space determined by these four amino acids is not conserved in human sirtuins. Compound **5** represents a new class of selective ligands with antileishmanial activity.

Introduction

Leishmaniasis is a vector-borne parasitic disease caused by protozoa of the genus Leishmania (Kinetoplastida, Trypanosomatidae). It is transmitted by the bite of female sand flies (Insecta, Diptera, Phlebotomidae). These parasites have two stages in their life cycle: the amastigote and the promastigote. The first is an intracellular form located in the vertebrate host, and the latter is a flagellate stage found in the sand fly. The medical condition ranges from cutaneous injuries to visceral, which is mortal if left untreated. Leishmaniasis is a neglected tropical disease that remains a burden in 97 countries where 350 million people are estimated to be at risk. Approximately 12 million people are infected worldwide and 0.7-1.0 million new cases occur annually (50,000-90,000 visceral leishmaniasis cases). The visceral form of the disease claims 26,000-65,000 lives every year. 1,2 Visceral leishmaniasis is caused by Leishmania (L.) donovani and L. infantum species. L. infantum (syn L. chagasi) is the only species identified as a causative agent of both visceral and cutaneous disease.3 Furthermore, this species has recently been identified as a causative agent of mucocutaneous and mucosal leishmaniasis.4 Whereas in visceral leishmaniasis, the parasite proliferates in the bone marrow, the liver and the spleen, in cutaneous diseases, parasites remain in the inoculation site, causing long-term skin ulcers that usually lead to disfiguring lesions. Although leishmaniasis due to L. donovani is an anthroponosis, L. infantum is responsible for zoonotic leishmaniasis, of which the dog is the main reservoir host.^{1,3,5} High prevalence rates of canine leishmaniasis are typical in endemic areas and represent an important risk factor for the emergence of the disease in humans.⁵ Outside America, cutaneous leishmaniasis is mainly due to parasites of *L. tropica* and *L. major* species.¹

Known drugs that are currently use to manage leishmaniasis have various problems, including high toxicity, adverse effects, resistance and high cost. Pentavalent antimonials, more often meglumine antimoniate, have been the treatment of first choice for decades despite of their high toxicity and the emergence of resistance. Nanoparticles and liposomal formulations may enhance drug effectiveness and safety. The current widespread use of the lipid formulation of amphotericin B in southern Europe and the Indian subcontinent, where antimonials have been replaced, highlights the advantages of new drug delivery systems. However, these amphotericin B liposomal formulations also have limitations: they are expensive, require a cool chain and slow infusion administration and hospitalization. Miltefosine was the last drug incorporated into the therapeutic options against leishmaniasis and the first oral drug available. However, it is not exempt from problems such as teratogenicity and drug resistance. Pentamidine and paromomycin are considered second-line therapies.

New investigations to develop less toxic drugs or more efficient therapeutic regimens are considered globally important and socially critical in certain research areas. Although several strategies could be undertaken to find new anti-infective treatments, one approach focuses on drug targets extensively investigated in human diseases. This information may be redirected for the investigation on parasitic diseases. One of these areas is epigenetics, where histone deacetylase (HDAC) inhibitors are being developed for a variety of human pathologies. This strategy is called the piggyback approach and uses the currently available information from human HDACs for antiparasitic drug development. 13,14

Vorinostat (1, Figure 1) is a pan-HDAC inhibitor that has been approved for the treatment of cutaneous T-cell lymphoma. ^{15,16} It has been used as a model to obtain analogs useful for a variety of human diseases ¹⁷ including infectious diseases (2-4, Figure 1). ^{18,19} Vorinostat displays

some antiparasitic activity over *Leishmania*. ^{19,20,21} Thus, this drug was chemically modified, aiming at improving the selectivity toward *Leishmania* in human cells.

Figure 1. Hydroxamate-based HDAC inhibitors

Several factors must be considered when developing an HDAC inhibitor as a drug for parasitic diseases, including a high level of selectivity for parasites versus host cells. ¹⁴ Consequently, several efforts have been described in the literature to improve the structure-activity relationships of hydroxamate-based HDAC inhibitors with antileishmanial activity (**3**, **4**, Figure 1). ²² HDAC inhibitors that belong to the hydroxamate class have often been considered devoid of activity if *O*-alkylation is present (both in human and nonhuman HDAC inhibitors), and the *O*-alkyl analogs have not been reported to be useful as antiparasitic drugs. However, *O*-modified hydroxamates with aromatic moieties would make it possible to target an aromatic cluster on the parasitic HDAC, thus increasing the affinity by π - π interactions. ²³ This particular modification could improve the selectivity for the parasite enzyme. We herein describe *O*-alkyl hydroxamate derivatives that display potent and selective *in vitro* and *in vivo* activity against *Leishmania*.

Results and discussion

Chemistry

The synthesis of hydroxamates has been described using a variety of methods^{24,25,26} including the functionalization of the molecule using *O*-protected hydroxylamine and deprotection of the obtained *O*-protected hydroxamic acid.^{27,28,29} Following this strategy, compounds **5-11**

were obtained (Figure 2). Compound **6** has been previously described, but it was not biologically evaluated against *Leishmania*.³⁰

Figure 2. Compounds synthesized

O-alkyl hydroxamates **5** and **6** were prepared following a modification of the procedure reported for vorinostat (Scheme 1).³¹ The use of *O*-alkyl hydroxyl amine after the activation of the acid affords the corresponding *O*-alkyl hydroxamate. This protocol was equally effective during the synthesis of **10** and **11** (Figure 2) starting from different acids. Compound **5** was also obtained using a standard protocol with the coupling reagent 1-ethyl-3-(3-dimethylaminopropyl)carbodiimide (EDCI) and the additive 1-hydroxy-7-azabenzotriazole (HOAt).³² However, the protocol using ethyl chloroformate proved to be useful during the synthetic scale-up.

OH
$$\frac{a) \text{ CICOOEt, TEA, 0 °C}}{b) \text{ NH}_2\text{O-R, dioxane, rt}}$$

$$5 \text{ R} = \text{C(Ph)}_3$$

$$6 \text{ R} = \text{CH}_2\text{Ph}$$

Scheme 1. The synthesis of O-alkyl hydroxamates

A different protocol was devised for the synthesis of the analogs **7-9** (Scheme 2). Vorinostat (1) was derivatized using the corresponding substituted commercially available chlorotrityl compounds in basic media.

Scheme 2. Synthesis of trityl analogs

Compound **5** was incorporated on the surface of both poly(lactic-co-glycolic acid) (PLGA) and gold nanoparticles. This was followed up by electrophoretic mobility measurements (see Supporting Information). From the electrophoretic point of view, any change in the electrophoretic mobility of both systems can be associated with the adsorption of **5** on the surface of the particles. To avoid gold nanoparticle aggregation, the free surface sites that remained uncovered by **5** were blocked with serum albumin.

Biological evaluation

The biological evaluation of compounds **5-11** (Figure 2) was conducted against *L. infantum* (Table 1). The results show an improvement of the antileishmanial activity of the trityl analog **5** compared to vorinostat (**1**, Figure 1). Compound **5** did not display cytotoxic activity as expected.

Table 1. Antileishmanial activity against *Leishmania infantum* intracellular amastigotes and cytotoxicity (CC_{50}) on mammal cells.

Compound	IC ₅₀ (μM) ^a	СС _{50 ВМДМ} (μМ) ^b	CC _{50 L929} (μM) ^c	
5	3.21 ± 1.2	>100	>100	
6	0.44 ± 0.03	>100	>100	
7	74.9 ± 21.0	>100	ND ^e	
8	69.1 ± 6.2	<100	ND	
9	ND	<1	<1	
10	3.67 ± 4.9	>100	ND	
11	1.05 ± 0.1	>100	>100	

Vorinostat	6.3 ± 3.8	5-20	ND		
PI ^d	1.50 ± 0.1	5-20	6.08 ± 0.2		
MA ^d	144.40 ± 41.0	200-500	273.08 ± 12.2		

⁽a) IC₅₀ against intracellular amastigotes of *L. infantum*

- (b) CC₅₀ on bone marrow-derived macrophages (BMDM)
- (c) CC₅₀ on L929 cells
- (d) Antileishmanial reference drugs: pentamidine isethionate (PI), meglumine antimoniate (MA)
- (e) ND: Not determined

Moreover, the antiparasitic activity was retained over the morphological stage of *L. infantum* amastigote, while no activity was observed against *L. infantum* promastigotes at 100 μ M. Compound **5** was potent against *L. infantum* amastigotes in a dose-dependent manner, and a mathematical model could be fitted where a positive relationship between its concentration and the percentage of infection reduction was found. Compounds **6** and **11** (Figure 2) were also potent against *L. infantum* intracellular amastigotes (Table 1) without showing activity against promastigotes. This result is in good agreement with the fact that the parasite HDAC isoforms are different depending on the parasite stage.^{33,34}

It should be noted that these results encompass a reverse structure-activity relationship with respect to the largely referenced fact that the hydroxamate class of potent human HDAC inhibitors do not show an oxygen substitution.^{35,36} Although there are exceptions to this trend,³⁷ it could provide access to new antiparasitic drugs with no activity against mammal cells because of shape differences and minimal amino acid residue changes in the target enzyme.

The *O*-trityl moiety in compound **5** is known as an acid-labile protecting group.³⁸ To check the importance of this chemical property in the antileishmanial activity, *O*-alkyl derivatives with different acid sensitivities were synthesized (**6-9**, Schemes **1** and **2**),^{39,40,41} with compound **6**

being the most acid-stable.³⁸ Compounds **7** and **8** failed to display antileishmanial activity (Table 1). Compound **9** displayed some cytotoxicity properties. However, compound **6** did show higher potency against *Leishmania* (and no cytotoxicity against mammal cells³⁰), also providing clear evidence that the *O*-alkyl hydroxamates could be valuable compounds as antileishmanial drugs.

The above results indicate that the *O*-alkyl vorinostat analogs, while devoid of any activity over mammal cells within the range of concentrations used, still retain potent *in vitro* antileishmanial activity. Thus, two unrelated trityl analogs were tested for antileishmanial activity (**10**, **11**, Figure 2). These compounds were obtained as a result of two independent programs for the synthesis of hydroxamic acids that were human HDAC inhibitors (unpublished results). Both compounds **10** and **11** displayed *in vitro* activity against *L. infantum*, suggesting the inclusion of *O*-alkyl hydroxamates in medicinal chemistry programs for evaluation as antiparasitic drugs.

As shown in Table 2, compound 5 was very potent against other *Leishmania* species as well; interestingly, 5 was three times more potent against the dermotropic species (*L. tropica* and *L. major*) than against the viscerotropic species (*L. infantum* and *L. donovani*). Differences in the *in vitro* drug sensitivities among *Leishmania* species is a well-known fact that has been reported for current antileishmanial drugs. Table 2 shows that the selectivity indices (SI) were higher than the value usually required to progress to the *in vivo* evaluation of candidate compounds (SI >10). 44

Table 2. Activity of compound **5** and the antileishmanial reference drugs pentamidine isethionate (PI) and meglumine antimoniate (MA) against viscerotropic and dermotropic *Leishmania* species. The mean ± standard deviation is shown.

5		MA		PI		
IC ₅₀ (μM) ^a	SI ^b	IC ₅₀ (μM) ^a	SI ^b	IC ₅₀ (μM) ^a	SI ^b	

L. infantum	3.21 ± 1.2	>31	144.4 ± 41	2	1.50 ± 0,1	4
L. donovani	2.91 ± 0.2	>34	96.4 ± 7	3	0.88 ± 0.2	7
L. major	1.00 ± 0.3	>100	101.1 ± 12	3	0.96 ± 0,2	6
L. tropica	0.71 ± 0.2	>140	123.3 ± 6	2	0.62 ± 0,1	10
CC ₅₀ (μM) ^c	>100	-	273.1 ± 12	-	6.08 ± 0.2	-

- a) Intracellular amastigote
- b) Selectivity Index (CC_{50,L929}/IC_{50,Leishmania})
- c) Cytotoxicity, cell line L929

Once the antileishmanial *in vitro* activity and selectivity was confirmed, compound **5** (Figure 2, Scheme 1) was selected for *in vivo* assays. Compounds **6**⁴⁵ and **11** were not included in this *in vivo* investigation since docking results showed that they could behave like vorinostat (see drug-target discussion below); thus, they could not function as an optimal selective antileishmanial drug.

Compound **5** (water solubility < 0.1 mg/mL) showed to be insoluble in plasma, which prompted the incorporation of **5** on PLGA nanoparticles or gold nanoparticles. These two materials were selected based on their compatibility with the host organism according to *in vivo* studies. 46,47,48 Previous to the *in vivo* investigation, these two formulations were assayed *in vitro* against *L. infantum*. Importantly, the *in vitro* reduction percentages of parasitic load were $54 \pm 9\%$ (**5** on PLGA nanoparticles at 3.21 μ M) and $71 \pm 1\%$ (**5** on gold nanoparticles at 14.3 μ M). Its activity was not significantly different (p>0.1) from that of free **5**, and no cytotoxicity was observed in these *in vitro* experiments with the supported drug. Thus, both **5** on PLGA nanoparticles and **5** on gold nanoparticles retained potency against *Leishmania* amastigotes *in vitro* and provided the solution for the *in vivo* administration. Free nanoparticles had no effect on the macrophage infection level. No toxic effects on macrophages were found with free nanoparticles either.

Toxicity tests carried out on infected mice confirmed the lack of toxicity of **5**. There were no plasma or serum biochemical or enzymatic value alterations or weight loss. The spleen, liver and kidney were not swollen, and they did not show any histological tissue disruption. On the other hand, mice treated with the antileishmanial reference drug (meglumine antimoniate) showed slightly higher aspartate aminotransferase (AST) values in comparison to those of untreated mice (p<0.05), suggesting liver damage, as previously reported.⁴⁹ However, mice treated with the drug combination (meglumine antimoniate and **5**, see Figure 3) using two different concentrations of **5** did not show any signs of toxicity, also providing evidence of the suitability of this drug combination. No toxicity effects were observed in healthy mice treated with a single dose of **5** supported on gold nanoparticles (500 mg/kg) or in the subacute toxicity experiment. These results were in accordance with the *in vitro* selectivity displayed by unsupported **5**.

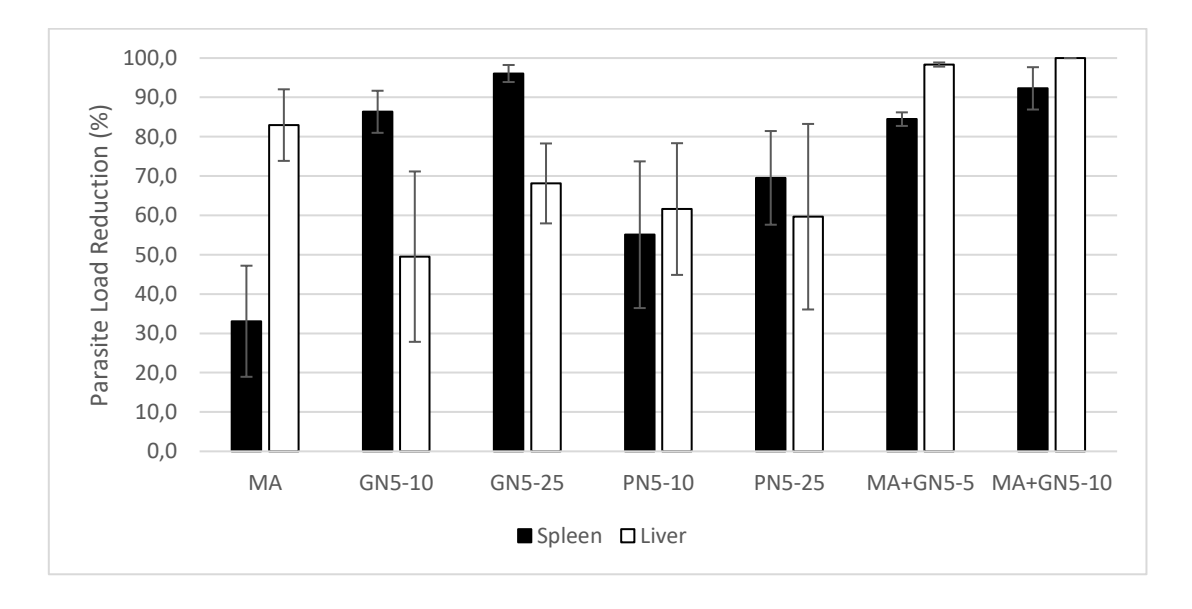


Figure 3. Parasite load reduction in spleen and liver from infected BALB/c mice. The Figure shows the average reduction of every treatment in percentages. MA= Meglumine antimoniate at 104 mg SbV/kg; GN5-10= 10 mg **5**/kg supported on gold nanoparticles; GN5-25= 25 mg **5**/kg supported on PLGA nanoparticles; PN5-25= 25 mg **5**/kg supported on PLGA nanoparticles; MA+GN5-5= Combination of meglumine antimoniate at 104 mg SbV/kg and 5 mg **5**/kg supported on gold nanoparticles; MA+GN5-10=

Combination of meglumine antimoniate at 104 mg SbV/kg and 10 mg **5**/kg supported on gold nanoparticles.

The experimental infections in mice were successful, accounting for high parasite loads in the spleen and liver of the animals and the isolation of the parasite in those organs and the bone marrow. The use of quantitative real-time PCR (qPCR) for the evaluation of antileishmanial compounds has been previously reported to estimate the parasite load in tissues and organs of infected laboratory animals. Some authors have recommended this technique to overcome the main disadvantages of classical methods (poor sensitivity and nonhomogeneous distribution of the amastigotes in the imprints). The *in vivo* intraperitoneal administration of **5** on gold nanoparticles to infected BALB/c mice confirmed to be effective at reducing the parasite load in the organs of infected mice, as shown in Figure 3. A significant reduction in *Leishmania* infection was observed after 14 days of treatment.

Treatment with the reference drug meglumine antimoniate⁴⁹ was very effective in the liver as it reduced the parasite load (83% reduction, p=0.0457), but it was not effective in the spleen since the parasite load reduction was not statistically significant (33% reduction, p>0.1). These results are in agreement with other authors who reported the low activity of meglumine antimoniate in the spleen of infected mice.^{52,53,54} In this infection model, the mean spleen parasite load is usually much higher than the mean parasite burden in the liver, in our case, 1571 parasites/mg and 470 parasites/mg, respectively. Conversely, the effectiveness of 5 supported on gold nanoparticles was very high in the spleen, at 10 mg/kg (86% reduction, p=0.0268) and 25 mg/kg (96% reduction, p=0.0025); the latter was even more effective than the treatment with the reference drug (p=0.0268). Compound 5 supported on gold nanoparticles at 25 mg/kg reduced parasites by 68% in the livers of infected mice, but this difference was not statistically significant (p=0.0701). Additionally, compound 5 supported on PLGA nanoparticles displayed less effectivity than the formulation with gold nanoparticles: at 10 mg/kg, the parasite load reduction was not significantly lower than the control (p>0.05). At

25 mg/kg, compound **5** decreased the spleen parasite load (70% reduction, p=0.0134), but the parasite burden decrease in the liver was not significantly different from that of the control (60% reduction, p=0.0890). The vehiculization of **5** on PLGA nanoparticles was discarded in favor of gold nanoparticles. This difference in activity can be associated with the size of the particles, as the gold cores are approximately seven times smaller than the PLGA particles. It is important to note that empty nanoparticles (PLGA and gold) had no impact on the parasite load of mice. Animals that were administered only saline solution or free nanoparticles were included in the experiments to assess the effect of free nanoparticles on the parasite load. There was no difference between these two groups of mice.

The combination of compound **5** supported on gold nanoparticles and meglumine antimoniate showed outstanding results since a clear improvement was detected, leading to a high parasite burden reduction in the two organs evaluated (Figure 3). Combining meglumine antimoniate and compound **5** at 5 mg/kg decreased the parasite load in the spleen (84% reduction, p=0.0009) and in the liver (98% reduction, p=0.0010). At 10 mg/kg, the parasite load reduction increased to 92% in the spleen (p=0.0008) and 100% in the liver (p=0.0012), leading to parasite clearance in this organ. In addition, these combinations were significantly more effective than the antimonial drug in monotherapy (p<0.05). The World Health Organization (WHO) recommends the use of combination therapy in visceral leishmaniasis in order to improve treatment efficacy, decrease the duration and cost of the therapy, reduce the occurrence of adverse effects and prevent the emergence of drug resistance. The latter is particularly relevant in the case of antimonials, the first-line drugs that are not currently used in some regions of India due to resistance.

These results prove for the first time that therapy with *O*-alkyl hydroxamates is effective against visceral leishmaniasis in a murine model. A structure–activity relationship study of bisnaphthalimidopropyl (BNIP) polyamine compounds concerning their activity against human SIRT1 and the parasitic enzyme Li-SIR2RP1 has been reported.^{56,57} A molecular docking study

showed a different molecular interaction of the most potent BNIP analog with the parasitic and the human enzyme, which could explain the observed selectivity of BNIPs. In our case, a more in-depth investigation should be conducted to probe the target of the *O*-alkyl hydroxamates, which could explain the described selectivity for the parasitic cells over the mammalian cells. From previous results,³⁶ the loss of the interaction with mammal Zn²⁺-dependent deacetylases may clarify that *O*-alkyl vorinostat analogs do not interfere with mammal cells.

An *in vitro* metabolite profiling of compound **5** was also conducted. The results show that vorinostat was not produced in the human hepatic microsomes. Three metabolites were identified by LC-MS/MS (Figure 4). Maximum metabolite formation was observed at 30 min of incubation, yielding metabolites **12** and **13** as having the strongest signals. These observations indicate that the main hepatic biotransformation routes take place through oxidations and cleavage of the hydroxamic moiety. The third metabolite (**14**) is the result of *N*-oxidation on the amide fragment. None of these results support that compound **5** might be a prodrug of vorinostat.

Figure 4. Metabolite profiling of compound 5.

Drug discovery programs include early assays for clearance determination of new compounds to avoid pharmacokinetic problems in more advanced stages.⁵⁸ Clearance of compound **5** is determined by its metabolic stability evaluation in human liver microsomes.⁵⁹ The study indicates that compound **5** displays a half-life value equal to 8.7 min. Consequently, the predicted intrinsic clearance calculated for this compound (see experimental section) was

established as 113.06 µL/min/mg protein. According to the classification bands used for classifying compounds into low, medium or high clearance,⁶⁰ compound **5** can be classified as having high clearance in human liver microsomes. Excluding prodrugs, compounds that show very high clearance are not considered optimal because they are presumably being cleared fast in vivo, leading to a short duration of action. However, the *in vivo* results in mice proving the antileishmanial activity of compound **5** supported on gold nanoparticles likely indicate a different metabolic pathway of the supported drug. The reduced clearance of several drugs using nanoparticles has been previously reported.⁶¹

Since combination therapies are considered advantageous for the treatment of leishmaniasis, pharmacokinetics with potential partner drugs such as meglumine antimoniate need to be evaluated. An *in vitro* cytochrome P450 inhibition evaluation was conducted (Table 3). The inhibition of CYP450 by compound 5 could influence the metabolism of the partner drug. From previous works, it has been concluded that if the *in vitro* inhibitory potency was $\leq 1~\mu$ M, an *in vivo* drug-drug interaction (DDI) would be observed; however, if the inhibitory potency was >10 μ M, there still is a remote possibility that the drug could cause an *in vivo* interaction.⁶² From the relevant CYP3A4 IC₅₀ and CYP2C9 IC₅₀ (Table 3), the *in vivo* evaluation of DDI is required for compound 5. In this regard, the antileishmanial activity observed *in vivo* (see above) with the combination of compound 5 and meglumine antimoniate is excellent, showing that the combination of both compounds represents a good therapeutic alternative.

Table 3. CYP450 inhibition for compound **5**.

CYP450	IC ₅₀ (μM)	Category		
CYP3A4	5.56	Moderate		
CYP2D6	>86.2	Weak		
CYP2C9	2.52	Moderate		

A cardiotoxicity study of compound **5** on HEK-293 hERG cells was also conducted. One of the main reasons for drug withdrawal is the drug-induced life-threatening arrhythmia

accompanying the prolongation of the QT interval in the electrocardiogram. The interaction with the potassium channel encoded by the human $ether-\dot{a}-go-go$ -related gene (hERG) has been identified as an important mechanism responsible for drug-induced prolongation of the QT interval in humans. In this sense, compound **5** presented low activity with an IC₅₀ of 96.22 μ M. This value is above the 10 μ M limit that has been reported as a preclinical IC₅₀ cutoff to not cause a QT increase. However, a higher cardiac risk has been reported for other antileishmanial drugs due to an increase in cardiac calcium currents. Thus, a study including other cardiac channels should be conducted to determine whether any safety issue could be developed when using O-alkyl vorinostat analogs $in\ vivo$.

Finally, compound **5** was analyzed for its mutagenic properties using the Ames test.⁶⁷ A compound that induces genetic mutations will likely cause cancer in humans.⁶⁸ The data were obtained for this compound using *Salmonella (S.) typhimurium* TA98 and *S. typhimurium* TA100, both in the absence of S9 metabolic activation. The results were compared with two positive controls, which are mutagenic and suspected to be carcinogenic agents (sodium azide and 2-nitrofluorene). The TA98 strain is used for the detection of frameshift mutations, while TA100 is used for base-pair substitutions. Table 7 and Figure 4 in the Supporting Information show the data obtained for **5** using *S. typhimurium* TA98. Table 8 and Figure 5 in the Supporting Information show the data obtained for **5** using *S. typhimurium* TA100. The data obtained afford evidence that compound **5** (75-10 μM) was not mutagenic and that this compound does not contain base-pair or frame-shift mutagens under the experimental conditions used in the present study.

Drug-target discussion

The specific HDAC isoform responsible for the antileishmanial activity in *L. infantum* for the above assayed compounds remains unknown. However, several HDAC inhibitors have been evaluated with promising responses, suggesting a key role of HDACs in parasitic survival, thereby emerging as a potential therapeutic target.^{69,70} To gain insight into the interactions

with these protein targets, a molecular docking investigation was conducted on selected Leishmania HDACs.

It has been reported that Leishmania genes encode four HDAC isoforms belonging to class I/II (Zn²⁺-dependent) and class III (NAD⁺-dependent, sirtuins). Both Zn²⁺- and NAD⁺-dependent HDACs have been suggested as molecular targets of classical pan-HDAC inhibitors. Referenced examples include vorinostat or trichostatin (for Zn²⁺-dependent HDACs)^{19,21} or sirtinol (for sirtuins). 71,72 However, no HDAC pertaining to class I or II has been structurally characterized in Leishmania. 21,34 To date, there is only gene information that allows us to infer by homology the possible HDAC protein sequence. Consequently, a primary HDAC protein sequence was retrieved from the UniProt database (code: A4HZ67), which could belong to a class I HDAC according to sequence similarities (see Supporting Information, Figure 9A; hereafter referred to as LiHDAC-I). Further, homology modeling to obtain a tridimensional (3D) model of LiHDAC-I was generated using the I-TASSER server⁷³ (https://zhanglab.ccmb.med.umich.edu/I-TASSER/; see Supporting Information, Table 9, Figures 7 and 8). Recently, a crystal structure of the deacetylase Leishmania infantum Silent Information Regulator 2 related protein 1 (LiSIR2rp1, PDB code: 5OLO⁷⁴) was reported. Since previous reports highlight the differential expression of the HDAC superfamily in amastigotes of *L. infantum*, 34,69,75 the NAD+-dependent deacetylase LiSIR2rp1 was also included in the docking calculations. Hence, compounds 5, 6, 10, 11, and vorinostat were submitted to docking in both enzymes (LiHDAC-I and LiSIR2rp1).

According to the docking studies (Figure 5), most of the compounds displayed a better binding affinity for both LiHDAC-I and LiSIR2rp1 than did vorinostat (Table 4), which agrees with the experimental *in vitro* antileishmanial activity observed. Compounds **5**, **6**, **10**, and **11** showed a greater affinity for LiSIR2rp1 than for LiHDAC-I. Thus, these ligands could inhibit both LiHDAC-I and LiSIR2rp1 with different potency.

Vorinostat reproduces the typical binding mode described for other HDACs⁷⁶ in LiHDAC-I (Figure 5D). The hydroxamic functional group interacts with Zn²⁺ and forms hydrogen bonds

with H155 and H192. In addition, the aliphatic linker of the compound was inserted in the tunnel, and the cap of the compound was accommodated at the surface of LiHDAC-I by hydrophobic interactions, π - π interactions with F219, and π -cation interactions with K214 (Figure 5D, Table 4).

Compounds **5**, **10** and **11** do not reach Zn^{2+} at the LiHDAC-I catalytic site (Figure 5, A-C); instead, they block the entry to the catalytic site and establish hydrophobic interactions with residues belonging to the surface cap region. The trityl moiety of compounds **5** and **10** makes π - π interactions with the side chain of H43, F164 and F220. Compound **11** blocks the entrance with the 4-butyl phenyl chain, creating π - π interactions (with F164, F220, and F119), π -cation interactions (with K214), and a hydrogen bond (with S218). Neither the phenyl alkyne of **10** nor the aromatic ring of **5** was found to be inserted into the catalytic tunnel of the HDACs. Instead, compound **10** projects out the phenyl alkyne chain and accommodates it between loop 1 and loop 2 of the protein. Compound **5** orientates its terminal aromatic ring like vorinostat, but without Zn^{2+} coordination. Compound **11** inserts its aliphatic chain (free of bulky groups) into the catalytic tunnel, resembling the aliphatic portion of vorinostat.

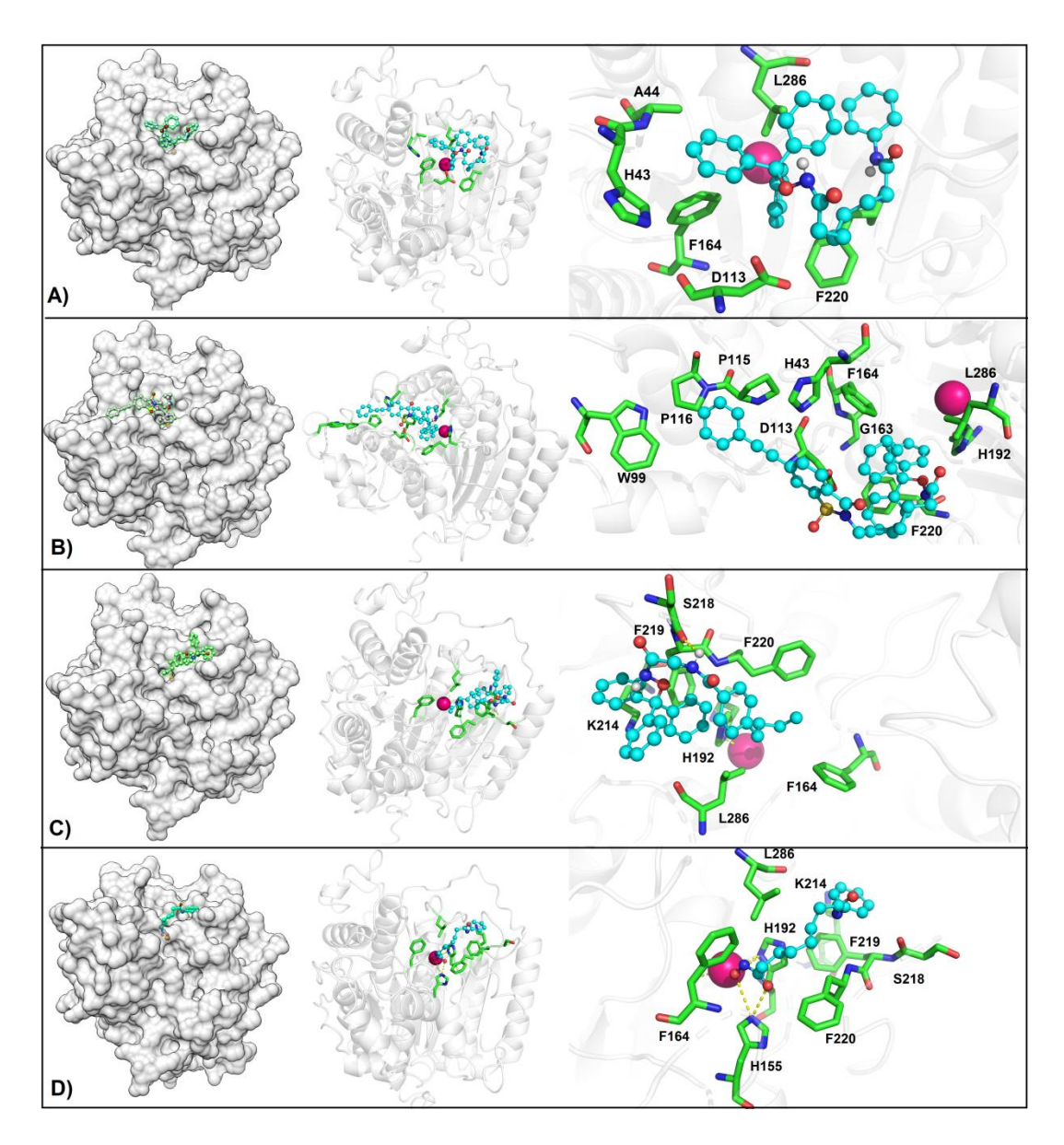


Figure 5. Noncovalent interactions of compounds **5** (A), **10** (B), **11** (C), and vorinostat (D) with LiHDAC-I (obtained from I-TASSER server; as the starting point, the following PDB IDs were used: 4A69, 4BKX and 4LY1). From left to right: First column, LiHDAC-I is depicted in surface representation with ligands shown in ball and stick representation. Second column, LiHDAC-I is depicted in cartoon representation, and the interacting residues are depicted as green sticks. Zn²⁺ is the pink sphere, and the ligand is in blue ball and stick representation. Third column, a zoom in on the interacting residues represented as green sticks with the ligands shown as blue balls and sticks. Hydrogen bonds are represented as yellow dotted lines.

Through these results, it was found that LiHDAC-I possesses an aromatic cluster at the entrance of the catalytic tunnel constituted by H43, F164, F219 and F220 that establishes hydrophobic and π - π interactions with the ligands (Table 4). This cluster is well conserved in human class I HDAC (see Supporting Information, Figure 9A). However, it should be highlighted that the surface residues V40, Q42, A44 (these three reached by compound 5), W99, G112, P116 (these three reached by compound 10), S218 (reached by compound 11), and F219 (reached by compound 11 and vorinostat) in LiHDAC-I are not conserved in human class I HDAC. Thus, these residues can be exploited to achieve selectivity among species (see Supporting Information, Figure 9A).

In addition to the above results, hydrophobic and π - π interactions were observed among the ligands (5, 6, 10, and 11) and LiSIR2rp1 (Figure 6). However, additional hydrogen bonding interactions explain the greater affinity of these compounds for LiSIR2rp1 than for LiHDAC-I. Three pockets in the LiSIR2rp1 active site have been described: A, B, and C. These pockets arise from the precise binding site of certain moieties in the cofactor NAD+ to the protein: a) in pocket A, the adenine-ribose portion is bound, b) in pocket B, the nicotinamide-ribose portion is bound, and c) pocket C is suggested as the nicotinamide binding site⁷⁷ (Supporting Information, Figure 10). To validate the docking protocol, the endogenous inhibitor of sirtuins, nicotinamide (NCA),⁷⁷ was also explored to reproduce its structural coordinates. NCA was found to bind to residues belonging to pocket C (S43, N125, I126 and D127), which agrees with previous reports,^{71,77} and to residues of pocket A (A40) and B (F51 and Q124) (Figure 6E).

Compounds **5**, **6**, **10**, and **11** display different behavior from that of NCA during recognition by the abovementioned pockets in the protein. For example, compounds **10** and **11** reach I126 from pocket C, exposing their trityl moiety outward. Compound **10** forms a hydrogen bonding interaction with R52, whereas compound **11** forms a π -cation interaction with R52. This interaction with R52 allows the ligands to be inserted deeply and reach I126 in pocket C (Figure 6, C-D). Regarding compound **6**, it was accommodated along the pockets A (A40), B (F51) and C

(l126), reaching the NAD⁺ binding site with a favorable free energy (-8.1 kcal/mol), even though only hydrophobic (F51 and L95) and π - π interactions (F74) were observed (Figure 6B). Finally, compound **5** reaches pockets A (A40, G41, V44, A45, N241, R242, and E243) and B (R52 and V221). The two carbonyl groups of compound **5** form hydrogen bonds with A40, R52, and S218 (Table 4, Figure 6A). Two facts should be highlighted for the interaction of compound **5** with LiSIR2rp1: a) it does not reach pocket C, which is conserved among sirtuin proteins, including human sirtuins;²¹ and b) it interacts with V44, A45, R242 and E243 in pocket A, which are semiconserved residues. Three of these amino acids (V44, R242 and E243) are also found in human SIRT1. However, the amino acid A45 is only found in human SIRT6 and SIRT7 (see Supporting Information, Figure 9B). It could be inferred that the lipophilic interactions that compound **5** establishes in pocket A with residues V44, A45, R242 and E243 might afford selectivity toward LiSIR2rp1. This consideration provides an opportunity for the compound to be a selective ligand while blocking the binding of the cofactor NAD⁺.

Vorinostat was bound to residues in pockets A, B and C in an overall similar way as that described for compound **6**. Additionally, vorinostat formed a hydrogen bond with D127, which was not observed in the interactions for **6** (Figure 6F and Table 4).

In summary, the four compounds investigated (**5**, **6**, **10**, and **11**) mainly establish three types of noncovalent interactions with LiSIR2rp1 (Table 4 and Figures 6A-D): a) hydrogen bonds with residues R52, S218, A40, I126, and D127; b) π - π interactions with a cluster of aromatic residues constituted by Y59, F74, H144, and F190; and c) hydrophobic interactions with several residues (A40-G41, S43-V44, I48-F51, L62, P70-W71, F74, L95, Q124-D127, H144, V187, F190, Q220-V221, N241-E243).

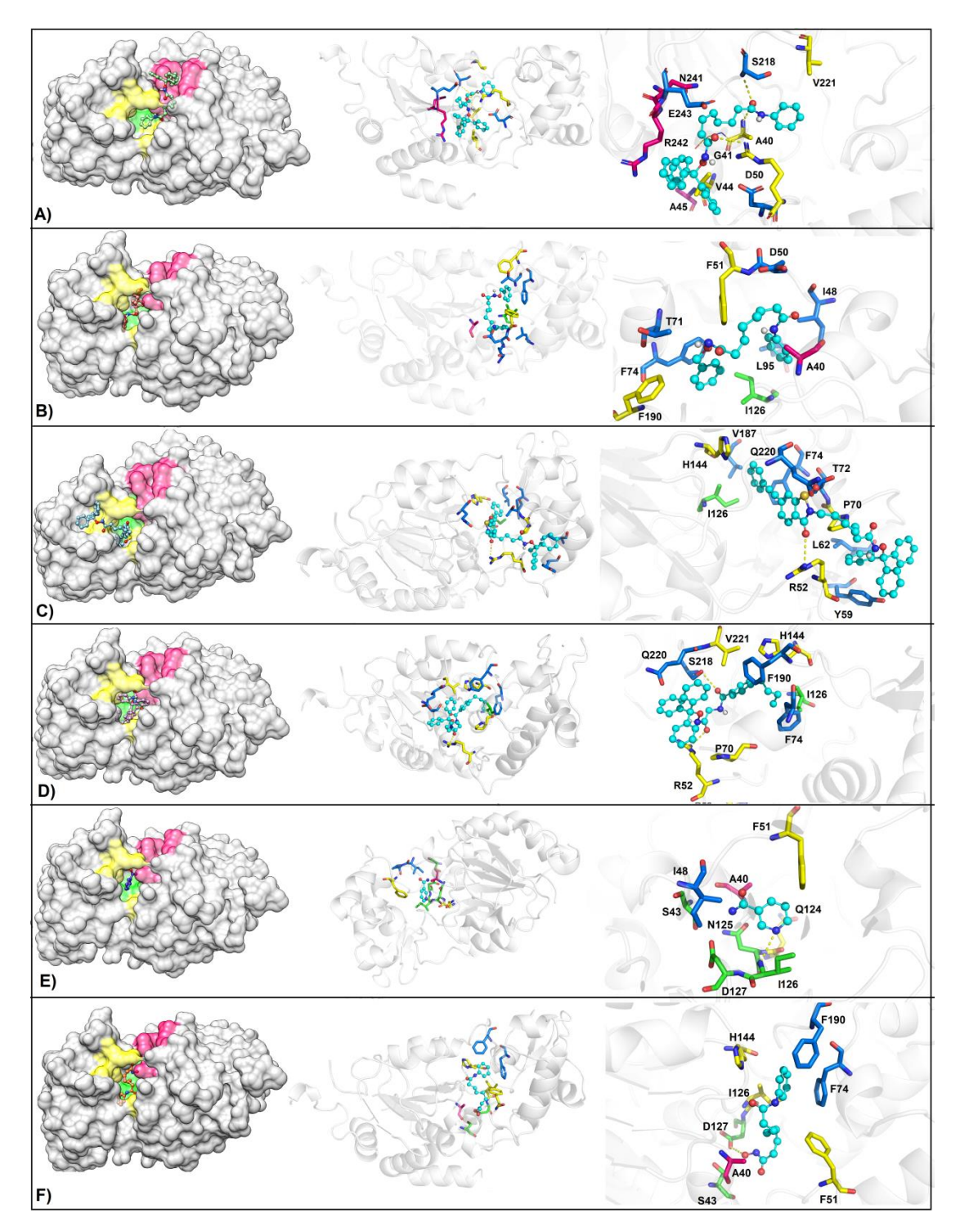


Figure 6. Docking results of **5** (A), **6** (B), **10** (C), **11** (D), nicotinamide (E) and vorinostat (F) on LiSIR2rp1 (PDB code: 5OLO⁷⁴). The first column on the left shows the surface representation of LiSIR2rp1 colored pink (pocket A), yellow (pocket B), and green (pocket C), while ligands are shown in ball and stick representation. The second column shows a gray cartoon representation of LiSIR2rp1 interacting with ligands (light blue) shown as blue balls and sticks, and the interacting residues are depicted as sticks colored according to the corresponding

pocket. The third column is a zoom in on the interaction between the ligand and the LiSIR2rp1 residues colored according to the corresponding pocket. Important residues in the second and the third column that did not belong to any pocket are colored marine blue.

Table 4. Docking simulation results between the selected compounds against the LiHDAC-I and LiSIR2rp1 models.

		LiH	DAC-I		LiSIR2rp1				
Ligand	Binding affinity (kcal/ mol)	HB ^{a,e}	π-π е	HP ^{b,e}	Binding affinity (kcal/ mol)	HB ^{a,e}	π-π °	HP ^{b,e}	
5	-6.8	ND^{d}	H43 (3.6), F164 (3.5), F220 (3.4)	A44 (3.7), D113 (3.5), L286 (3.5)	-7.2	A40 (3.3), A45 (4.0) R52 (3.3), S218 (3.3)	$\mathrm{ND^d}$	G41 (3.6), V44 (3.4), D50 (3.6), V221 (3.7), N241 (3.3), R242 (3.6), E243 (3.6)	
6	ND ^d	ND^{d}	ND^{d}	$\mathrm{ND^d}$	-8.1	$\mathrm{ND^d}$	F74 (3.8)	A40 (3.7), I48 (3.7), D50 (3.8), F51 (3.8), T71 (3.6), L95 (3.9), I126 (3.6), F190 (3.4)	
10	-7.0	$\mathrm{ND^d}$	H43 (3.7), F164 (4.0),	W99 (3.6), D113(3.9), P115 (3.7), P116 (3.6),	-7.4	R52 (3.3)	F74 (3.9), H144 (3.7), Y59 (4.0)	L62 (3.6), P70 (3.9), T71 (3.5), I126 (3.6), V187 (3.7), Q220 (3.6)	

			F220	G163 (3.5),						
			(3.7)	L286 (3.2),						
				H192 (3.0)						
	5.0	S218	F219	F164 (3.8), H192 (3.4),	(2)	R52 (3.1),	MDd	P70 (3.4), F74 (3.7), I126 (3.7),		
11	-5.9	-5.9 (2.5)			(3.4),	K214 (3.9), F220 (3.7), L286 (3.5),	-6.3	S218 (3.2)	$\mathrm{ND^d}$	H144 (4.0), F190 (3.6), Q220 (3.4), V221 (3.9)
Vorinostat	-5.4	H155 (3.4) (2.9), H192 (3.5)	F219 (3.7)	F164 (3.0), K214 (3.5), S218 (3.4), F219 (3.7), F220 (3.8), L286 (3.7), ZN	-6.5	D127 (3.5)	F74 (3.8), H144 (4.0), F190 (3.7)	A40 (3.7), S43 (3.6), F51 (3.6), I126 (3.7)		
NCA°	$\mathrm{ND^d}$	ND ^d	ND^{d}	ND^{d}	-3.9	I126 (3.4)	$\mathrm{ND^d}$	A40 (3.8), S43 (3.7), I48 (3.5), F51 (3.8), Q124 (3.7), N125 (3.4), D127 (3.6)		

- (a) Hydrogen bond
- (b) Hydrophobic interactions
- (c) Nicotinamide
- (d) Not detected
- (e) Bond distance in Å

Conclusions

O-Alkyl hydroxamic acids derived from vorinostat have displayed potent and selective in vitro activity against intracellular amastigotes of L. infantum and other Leishmania species. Other Otrityl hydroxamic acids also showed in vitro activity against L. infantum, prompting the idea of searching for specific drugs against leishmaniasis in libraries containing these derivatives. The O-trityl derivative of vorinostat, 5, supported on gold nanoparticles has proven in vivo activity in a mouse model of L. infantum infection. Importantly, the antileishmanial activity of 5 and meglumine antimoniate has been described in the same animal model. When co-administered, the antileishmanial activity was superior to that obtained in each individual treatment. For the first time, an O-alkyl hydroxamic acid derivative has been shown to be effective against visceral leishmaniasis in a murine model. The in vitro metabolite profiling results and in vitro activity of the analogs containing a modification of the trityl derivative indicate that vorinostat is not produced in vivo after the administration of 5. In silico studies have shown that the Osubstituted aromatic hydroxamic acids synthesized are capable of reaching aromatic clusters of parasitic LiHDAC-I and LiSIR2rp1, forming $\pi-\pi$ interactions. This finding could explain the biological properties of the compounds. Additionally, compound 5 does not establish interactions in pocket C of LiSIR2rp1 and interacts with key semiconserved residues (V44, A45, R242, and E243) in pocket A. This fact confers differences in the surface pocket that might affect the binding mode with human sirtuins. Thus, compound 5 opens the opportunity to obtain new selective ligands while blocking the binding of the cofactor NAD⁺ in LiSIR2rp1.

Experimental Section

General Procedures. Animals were purchased from Harlan Ibérica (Barcelona, Spain). L929 fibroblasts, properly identified (ECACC: 85011425), were acquired at the Cell Bank of the University of Granada. Reference drugs for the treatment of leishmaniasis, pentamidine isethionate (Pentacarinat®) and meglumine antimoniate (Glucantime®) were purchased from Sanofi-Aventis (Paris, France). Potassium phosphate buffer (100 mM) pH 7.4 and human liver microsomes were purchased from Beckton Dickinson. Verapamil and NADPH were purchased

from Sigma-Aldrich (Germany). Reaction or purification solvents and chemicals were used as purchased without further purification. Before the purification of the O-trityl derivatives, ethyl acetate was treated with an aqueous solution of NaHCO3. The organic layer was dried over MgSO₄, filtered, and used in flash chromatography as specified. Milli-Q-grade water was used for the preparation of all suspensions and solutions (Milli-Q Academic, Millipore, France). Reactions and purifications were monitored on Merck precoated silica gel plates (with fluorescence indicator UV254) using solvent systems based on ethyl acetate, n-hexane, dichloromethane, and methanol. Flash column chromatography was performed with silica gel 60 (230-400 mesh ASTM) and the specified solvent mixtures for each compound. Spots were visualized by irradiation with ultraviolet light (254 nm) or by staining with iodine or ninhydrin (0.2% solution in ethanol). Melting points (mp) were determined in open capillaries on an electrothermal melting point apparatus and are uncorrected. Proton (1H) and carbon (13C) nuclear magnetic resonance (NMR) spectra were recorded on a 300 MHz Varian Inova Unity, 400 MHz Varian Direct Drive, or 500 MHz Varian Direct Drive system using the stated deuterated solvent. Chemical shifts are given in parts per million (ppm) (δ relative to residual solvent peak for 1H and 13C). Coupling constants (J) are reported in hertz (Hz). High-resolution mass spectrometry (HRMS) analysis was performed using a time of flight (ToF) instrument (LCT Premier™, Waters). The samples were ionized after direct infusion by ES. The abovementioned instruments belong to the Scientific Instrumentation Center of the University of Granada. Liquid chromatography-mass spectrometry (LC-MS) analysis was performed using a single quadrupole system (Agilent 6110) equipped with electrospray ionization (ESI). The pump was a binary Agilent 1200, and the column was a Zorvax Eclipse XDB-C18, 5 µm particle size (150 mm × 4.6 mm). Eluent A was water with 0.1% formic acid; eluent B was acetonitrile (ACN) with 0.1% formic acid; a flow rate of 0.8 mL min⁻¹ was used; and samples were prepared in a H_2O/ACN (80:20) mixture, and filtered before injection. Compound purity was determined by high-performance liquid chromatography (HPLC). The purity of all final compounds was 95% or higher. The HPLC instrument (Agilent) was a quaternary 1200 pump equipped with a diode array detector (DAD), a thermostatted column compartment, an autosampler, and a vacuum degasser. The column was a Zorvax Eclipse XDB-C18, 5 μ m particle size (150 mm \times 4.6 mm). Eluent A was water with 0.1% formic acid; eluent B was ACN with 0.1% formic acid; the method was isocratic (70:30), gradient to 100% B for 20 min, isocratic B for 2 min; a flow rate of 0.8 mL min⁻¹ was used, with detection at 214 nm and 254 nm; and the column temperature was 25 °C. Samples were prepared in a H_2O/ACN (80:20) mixture, and filtered. When specified, irradiation by microwave was conducted on a Biotage Initiator Microwave instrument.

HPLC methods: (A) solvent A (H_2O :ACN 30:70 + 0.1% HCOOH), solvent B (ACN 100% + 0.1% HCOOH); isocratic solvent A 2 min; gradient from A to B 10 min; (B) solvent A (H_2O :ACN 40:60 + 0.1% HCOOH), solvent B (ACN 100% + 0.1% HCOOH); isocratic solvent A 2 min; gradient from A to B 20 min; (C) solvent A (H_2O :ACN 50:50 + 0.1% HCOOH), solvent B (ACN 100% + 0.1% HCOOH); isocratic solvent A 2 min; gradient from A to B 5 min; (D) solvent A (H_2O :ACN 70:30 + 0.1% HCOOH), solvent B (ACN 100% + 0.1% HCOOH); isocratic solvent A 2 min; gradient from A to B 13 min; and isocratic solvent B 5 min.

LC-MS methods: (E) solvent A (H_2O :ACN 90:10 + 0.1% HCOOH), solvent B (ACN 100% + 0.1% HCOOH); isocratic solvent A 2 min; gradient from A to B 15 min; (F) solvent A (H_2O :ACN 90:10 + 0.1% HCOOH), solvent B (ACN 100% + 0.1% HCOOH); isocratic solvent A 2 min; and gradient from A to B 10 min.

Equipment for metabolite profiling and identification: Agilent 1290 Infinity ultra high performance liquid chromatography (UHPLC), AB Sciex TripleTOF 5600 mass spectrometer.

Materials. Compound **1** was prepared according to known procedures.^{17,78,31} Compounds **7-9** were synthesized according to the procedure of Mai *et al* with the specified modifications.³¹ Gold nanoparticles were synthesized following the citrate thermal reduction method developed by Turkevich *et al*.⁷⁹ BMDMs were used as an infection model according to Zauli-Nascimento *et al*.⁸⁰

N-Phenyl-N'-(trityloxy)octanediamide (5)

Procedure A: The compounds 8-oxo-8-(phenylamino)octanoic acid (121 mg, 0.485 mmol), Otritylhydroxylamine (133 mg, 0.485 mmol, 2 equiv.), 1-hydroxy-7-azabenzotriazole (HOAt) (66 mg, 0.485 mmol, 2 equiv.), and 1-ethyl-3-(3-dimethylaminopropyl)carbodiimide (EDCI) (93 mg, 0.485 mmol, 2 equiv.) were dissolved in N,N-dimethylformamide (DMF) (1 mL). After triethylamine (TEA) (68 µL, 0.485 mmol, 2.0 equiv.) was added, the reaction was stirred at room temperature (r.t.) for 5 h. Then, the reaction was diluted with dichloromethane (30 mL) and washed with H_2O (3 x 15 mL) and brine (1 x 15 mL). The organic layer was dried over MgSO₄, filtered and evaporated. The residue was purified by flash chromatography, eluting with ethyl acetate/hexane (1:2) to afford product **5** (white solid, 106 mg, 43% yield). Procedure B: In a dry flask, a solution of 8-oxo-8-(phenylamino)octanoic acid (2 g, 8.02 mmol) in anhydrous THF (50 mL) was prepared at r.t. under an argon atmosphere. The solution was cooled at 0 °C and ethyl chloroformate (1.02 mL, 10.67 mmol) followed by TEA (2.24 mL, 16.04 mmol) was added dropwise. After stirring at 0-5 °C for 1.5 h, the reaction was allowed to warm at r.t over 20 min. The mixture was then filtered on a previously dried two-neck round bottom flask, which was then purged with argon before the addition of solid O-tritylhidroxylamine (3.754 g, 13.63 mmol). Stirring was maintained under argon for 20 h, after which the reaction was stopped by evaporation of the solvent under reduced pressure. The white residue was dissolved in acetone, filtered and washed with small volumes of water. The resulting white solid (5) was dried under vacuum at 35 °C, in the presence of NaOH (3.23 g, 6.38 mmol, 80%). $R_{\rm f}$: 0.15 (Ethyl acetate/hexane 1:2). Mp 175-177 °C. ¹H NMR (300 MHz, DMSO- d_6) δ 10.14 (bs, 1H), 9.80 (bs), 7.58 (d, J = 7.7 Hz, 2H), 7.39 – 7.20 (m, 17H), 7.01 (t, J = 7.4 Hz, 1H), 2.24 (t, J = 7.4 Hz, 2H), 2.24 (t, J = 7.4 7.4 Hz, 2H), 1.84 – 1.68 (m, 2H), 1.54 – 1.44 (m, 2H), 1.27 – 1.07 (m, 4H), 1.06 – 0.93 (m, 2H). 13 C NMR (75 MHz, DMSO- d_6) δ 171.14, 170.27, 142.43, 139.30, 128.92, 128.56, 127.45, 127.35, 122.84, 118.99, 91.70, 36.34, 31.93, 28.31, 28.14, 24.90, 24.65. HRMS (ESI): *m/z* calculated for $C_{33}H_{34}N_2O_3Na$ [M+Na]⁺ 529.2467, found 529.2462 (deviation -0.9 ppm). HPLC purity (method B, λ =254): 100%, t_R = 10.29 min.

N¹-(benzyloxy)-N²-phenyloctanediamide (6)

A solution of 8-oxo-8-(phenylamino)octanoic acid (50 mg, 0.20 mmol) in anhydrous THF (3 mL) was prepared under argon in a previously dried three-neck flask. The solution was cooled at 0 °C, and ethyl chloroformate (0.03 mL, 0.27 mmol) followed by triethylamine (0.1 mL, 0.70 mmol) was added dropwise. The mixture was stirred under argon at 0-5 °C for 1.5 h. After this time, the reaction was allowed to warm at r.t before the addition of solid O-benzylhydroxylamine hydrochloride (54 mg, 0.34 mmol). Stirring under argon at r.t. was maintained for 1.5 h, after which the reaction mixture was diluted with ethyl acetate and distilled water. After separation of the phases, the resulting organic layer was washed with distilled water (x3), dried over Na₂SO₄, filtered, and evaporated under vacuum. The white residue was purified by flash chromatography on silica (stepped gradient elution using mixtures of dichloromethane/methanol (10:0.1, 10:0.2, and 10:0.3) to afford 6 (white solid, 28 mg, 40% yield).

 $R_{\rm f}$: 0.27 (dichloromethane/methanol 10:0.5). Mp 130-131 °C. ¹H NMR (500 MHz, CD₃OD) δ 7.54 (m, 2H), 7.33-7.25 (m, 7H), 7.08 (m, 1H), 4.75 (s, 2H), 2.52 (m, 2H), 2.36 (m, 2H), 1.70-1.65 (m, 4H), 1.41 (m, 4H); ¹³C NMR (125 MHz, CD₃OD) δ 176.1, 174.6, 139.9, 138.0, 129.7, 129.5, 129.3, 128.5, 125.1, 121.3, 52.9, 37.9, 33.1, 30.1, 30.0, 26.8, 25.8; HRMS (ESI) m/z calculated for $C_{21}H_{27}N_2O_3$ [M + H]⁺ 355.2022, found 355.2025. HPLC purity (method D, λ =254): 100%, t_R = 11.14 min.

N-((2-Chlorophenyl)diphenylmethoxy)-N'-phenyloctanediamide (7)

 N^1 -Hydroxy- N^8 -phenyloctanediamide (10 mg, 0.038 mmol, vorinostat) was dissolved in dry DMF (1 mL), and Na_2CO_3 (8 mg, 0.075 mmol, 2.0 equiv.) and 2-chlorotrityl chloride (18 mg, 0.057 mmol, 1.5 equiv.) were added sequentially under an argon atmosphere. The reaction was stirred at 40 °C for 24 h. The mixture was diluted with H_2O (20 mL) and extracted with

ethyl acetate (3 x 15 mL). The organic layer was dried over MgSO₄, filtered and evaporated. The residue was purified by flash chromatography, eluting with ethyl acetate/hexane (3:2) to afford product **7** (white solid, 4 mg, 21% yield).

 $R_{\rm f}$: 0.43 (ethyl acetate/hexane 2:1). ¹H NMR (500 MHz, DMSO- $d_{\rm f}$) δ 10.07 (sa, 1H), 9.80 (s, 1H), 7.95 (d, J = 7.7 Hz, 1H), 7.58 (d, J = 7.7 Hz, 2H), 7.48 – 7.45 (m, 1H), 7.40-7.26 (m, 14H) 7.01 (t, J = 7.4 Hz, 1H), 2.24 (t, J = 7.4 Hz, 2H), 1.81 – 1.69 (m, 2H), 1.52 – 1.46 (m, 2H), 1.20 – 1.10 (m, 4H), 1.01 – 0.97 (m, 2H). ¹³C NMR (126 MHz, DMSO- $d_{\rm f}$) δ 171.62, 139.78, 131.97, 130.36, 130.34, 129.98, 129.93, 129.05, 128.02, 127.65, 127.49, 123.33, 123.29, 119.46, 119.36, 36.81, 32.45, 28.79, 28.59, 25.38, 25.10. HRMS (ESI): m/z calculated for $C_{33}H_{33}CIN_2NaO_3$ [M+Na]⁺ 563.2077, found 563.2070 (deviation +1.2 ppm). HPLC purity (method A, λ =254): 100%, $t_{\rm R}$ = 9.25 min.

N-(Diphenyl(p-tolyl)methoxy)-N'-phenyloctanediamide (8)

 N^1 -Hydroxy- N^8 -phenyloctanediamide (10 mg, 0.038 mmol, vorinostat) was dissolved in dry DMF (1 mL), and Na_2CO_3 (8 mg, 0.075 mmol, 2.0 equiv.) and 4-methyltriphenylmethyl chloride (17 mg, 0.058 mmol, 1.5 equiv.) were added sequentially under an argon atmosphere. The reaction was stirred at 40 °C for 24 h. The mixture was diluted with H_2O (20 mL) and extracted with ethyl acetate (3 x 15 mL). The organic layer was dried over MgSO₄, filtered and evaporated. The residue was purified by flash chromatography, eluting with ethyl acetate/hexane (1:1) to afford product **8** (white solid, 3 mg, 15% yield).

 $R_{\rm f}$: 0.38 (ethyl acetate/hexane 1:2). Mp 133-136 °C. 1 H NMR (500 MHz, DMSO- $d_{\rm f}$) δ 10.09 (s, 1H), 9.79 (s, 1H), 7.58 (d, J = 7.8 Hz, 2H), 7.32 – 7.26 (m, 12H), 7.19 (d, J = 7.8 Hz, 2H), 7.12 (d, J = 7.9 Hz, 2H), 7.01 (t, J = 7.4 Hz, 1H), 2.28 (s, 3H), 2.24 (t, J = 7.4 Hz, 2H), 1.81 – 1.74 (m, 2H), 1.52 – 1.46 (m, 2H), 1.20 – 1.11 (m), 1.04 – 0.96 (m, 2H). 13 C NMR (126 MHz, DMSO- $d_{\rm f}$) δ 171.13, 170.22, 142.66, 139.37, 139.30, 136.54, 129.04, 128.82, 128.57, 128.01, 127.41, 127.25, 122.84, 118.98, 91.61, 36.34, 31.97, 28.33, 28.12, 24.91, 24.64, 20.55. HRMS (ESI): m/z

calculated for $C_{34}H_{36}N_2NaO_3$ [M+Na]⁺ 543.2624, found 543.2617 (deviation +1.3 ppm). HPLC purity (method A, λ =254): 100%, t_R = 7.58 min.

N-(Bis(4-methoxyphenyl)(phenyl)methoxy)-N'-phenyloctanediamide (9)

N¹-Hydroxy-N³-phenyloctanediamide (20 mg, 0.076 mmol, vorinostat) was dissolved in dry DMF (1 mL), and Na₂CO₃ (48 mg, 0.453 mmol, 6.0 equiv.) and 4,4¹-dimethoxytrityl chloride (77 mg, 0.227 mmol, 3.0 equiv.) were added sequentially under an argon atmosphere. The reaction was stirred at 40 °C for 24 h. The mixture was diluted with H₂O (20 mL) and extracted with ethyl acetate (3 x 15 mL). The organic layer was dried over MgSO₄, filtered and evaporated. The residue was purified by flash chromatography, eluting with ethyl acetate/hexane (1:1) to afford product **9** (white solid, 28 mg, 64% yield). R_1 : 0.22 (ethyl acetate/hexane 2:1). ¹H NMR (300 MHz, DMSO- d_6) δ 10.07 (bs, 1H), 9.80 (bs, 1H), 7.58 (dd, J = 8.6, 1.1 Hz, 2H), 7.35 – 7.24 (m, 7H), 7.20 (d, J = 8.7 Hz, 4H), 7.03 – 6.99 (m, 1H), 6.86 (d, J = 8.8 Hz, 4H), 3.73 (s, 6H), 2.25 (t, J = 7.4 Hz, 2H), 1.85 – 1.73 (m, 2H), 1.55 – 1.45 (m, 2H), 1.26 – 1.12 (m, 4H), 1.08 – 0.94 (m, 2H). ¹³C NMR (75 MHz, DMSO- d_6) δ 171.13, 170.11, 158.37, 139.31, 134.46, 130.46, 128.56, 128.44, 127.45, 127.06, 122.84, 118.98, 112.69, 91.35, 54.99, 36.35, 32.00, 28.37, 28.18, 24.90, 24.66. HRMS (ESI): m/z calculated for C₃₅H₃₈N₂NaO₅ [M+Na]* 589.2678, found 589.2672 (deviation +1.0 ppm). HPLC purity (method

Synthesis of gold nanoparticles

A, λ =254): 96%, t_R = 5.51 min.

Briefly, a gold solution was prepared by adding 4.5 mg of sodium tetrachloroaurate (III) dihydrate to 25 mL of water.⁷⁹ The solution was boiled under reflux, and 1 mL of a 1% sodium citrate tribasic dihydrate solution was rapidly added via syringe into the boiling solution under vigorous stirring. The citrate ion acts both as a reagent and as a stabilizer of the growing gold particles. After boiling for 20 min, the solution was cooled to r.t. under magnetic stirring. The result of the synthesis is a stable dispersion of gold nanoparticles with an average

hydrodynamic diameter of 20 nm (coefficient of variation below 8%), as determined by dynamic light scattering (DLS) measurements.

Synthesis of PLGA nanoparticles

PLGA nanoparticles were synthesized following the water-in-oil-in-water (w/o/w) double emulsion/solvent evaporation method.⁸¹ Briefly, 3 mL of a 1% aqueous solution of dextran 70 was added dropwise to a 10 mL 2.5% PLGA solution in ethyl acetate with the help of a vortex. Under mechanical stirring (20·103 rpm), this emulsion was added dropwise into 50 mL of a 0.3% PVA aqueous solution. The resulting w/o/w emulsion was formed. After 25 min., the w/o/w emulsion was diluted in 100 mL of a 2% PVA solution. Finally, the stirring rate was reduced to 1000 rpm. The mechanical stirring was continued overnight with the aim of removing the organic solvent by evaporation. Several cycles of centrifugation and redispersion in distilled water were performed on a PLGA colloidal suspension with the aim of removing the secondary products that remained in the synthesis, until the conductivity of the supernatant was below 5 μS/cm.

Functionalization of gold nanoparticles with 5

In brief, 5-coated gold was prepared by adding 1 mL of the nanogold stock solution dropwise to 1 mL 5 solutions under vortexing. Compound 5 was previously dissolved in a 0.2% Triton X-100 solution at pH 6.5 with the help of ultrasound. The adsorption of compound 5 produced an easily observable change in the color of the suspension from red to blue/violet, indicating particle aggregation and increased average particle size. These observations were confirmed by DLS. Hence, with the aim of avoiding nanoparticle aggregation, a crucial step consists of functionalizing the 5-coated gold particles with a protective polyelectrolyte/polymer. Thus, bovine serum albumin (BSA) was used, and the 5-coated particles without further washing steps were added dropwise to a 1% solution of BSA.

The **5**-coated PLGA particles were prepared by adding 1 mL of a 1% (w/v) PLGA suspension dropwise to a 1 mL solution of **5** under vortexing. The **5** solution was prepared as previously described.

Electrical surface characterization-dynamic light scattering

The hydrodynamic diameter and electrophoretic mobility measurements were carried out using a Zetasizer Nano-ZS (from Malvern Instruments, UK). Electrophoretic mobility measurements were performed in diluted suspensions with fixed ionic strength (1 mM KNO₃) at different pH values. KOH (0.01 M or 0.1 M) and HNO₃ (0.01 M or 0.1 M) were employed to adjust the pH values of the suspensions. The suspensions were left unperturbed overnight, the pH was readjusted if needed and the electrophoretic mobility was then measured by performing 3 runs of 3 measurement cycles each.

Optical absorbance

Compound **5** water solutions (0.2 mL) at different concentrations (10⁻⁴-10⁻² M) were mixed with an aqueous solution of the final gold nanoparticles, and the mixtures were left under mechanical stirring overnight at r.t. After that time, the solutions were centrifuged (15 min; 16000 rpm). With the aim of determining the amount of **5** adsorbed on the surface of the gold nanoparticles, the absorbance of the **5**-gold supernatants was measured at 187 nm, and the absorbance was compared to that of the initial drug solution. Optical absorbance determinations were performed with a Dinko UV-8500 UV-Vis spectrophotometer (Dinko Instruments, Spain) using 1 cm path length quartz cuvettes.

Drug release determination

The drug release from drug-loaded particles was also measured spectrophotometrically: the particles were dispersed in RPMI-1640 (GIBCO-BRL, Invitrogen, USA) culture medium to a solids concentration corresponding to a volume of 1 mL from the mother solution. The particles were first kept in contact with a 0.01 M solution of 5 for 48 h; after this time, they were centrifuged and dispersed in the culture medium as described. At specified time

intervals, a 4 μ L aliquot was removed, and its absorbance at 190 nm was measured in an Implen Nanophotometer (Spectra Services, USA).

Biological evaluation

Parasite. For the *in vitro* and *in vivo* experiments two autochthonous isolates of *Leishmania infantum*, MHOM/ES/2007/DP532JFJ obtained from a local human visceral leishmaniasis case and MCAN/ES/2007/DP534 obtained from a local canine leishmaniasis case, were used. These strains were properly characterized through isoenzyme electrophoresis and identified as *L. infantum* MON-1. Both strains were isolated and characterized by the Parasitology research group. The *L. donovani* strain used, MHOM/IN/00/LEM138, was characterized through isoenzymed electrophoresis and identified as *L. donovani* MON-2. *L. tropica* (MHOM/MA/1988/LEM1314) and *L. major* (MRHO/SU/1959/LEM129) were also characterized through isoenzyme electrophoresis and identified as *L. tropica* MON-102 and *L. major* MON-4, respectively. The parasites were grown as promastigotes in RPMI-1640 medium supplemented with 10% heat-inactivated fetal bovine serum (FBS), and 200 U/mL penicillin at 24 °C. To maintain infectiveness, parasites with less than 10 *in vitro* passages were used to perform *in vivo* infections.

Animals. Swiss (ICR CD-1) mice of approximately 30 g weight were used as the source of BMDMs and for *in vivo* toxicity evaluation. Female BALB/c mice of approximately 18 g weight (4-6 weeks old) were used for *in vivo* experiments. Animals were handled in accordance with guidelines for Animal Experimentation recommended by the Federation for Laboratory Animals Science Associations (FELASA). They were properly housed under 12 h light cycles and provided with water and food *ad libitum*.

Antileishmanial compounds. Compounds were received as powder. For *in vitro* experiments, these compounds were diluted in dimethylsulfoxide (DMSO) and properly added to every well to obtain the intended final concentration with 0.5% DMSO in the medium. For the *in vivo* administration experiments, **5** was supported on PLGA or gold nanoparticles (see above) and

administered through an intraperitoneal route. The antileishmanial reference drugs for the *in vitro* experiments (pentamidine isethionate and meglumine antimoniate) were added to every well to the intended concentration. For the *in vivo* experiments, meglumine antimoniate was diluted with physiological saline solution to a maximum volume of 500 μ L and administered through an intraperitoneal route.

In vitro assays for biological evaluation.

Mammal cell cultures and culture media. L929 fibroblasts were grown in Roswell Park Memorial Institute (RPMI) 1640 medium supplemented with 10% fetal bovine serum (FBS) and 200 U/mL penicillin at 37 °C (5% CO₂). They were used both for obtaining L929 cell conditioned medium (LCCM), and for cytotoxicity assays. BMDMs were obtained as undifferentiated bone marrow cells from bone marrow of healthy Swiss mice. The cells were differentiated into macrophages, ⁸² by culturing them in RPMI-1640 supplemented with 20% FBS, 30% LCCM and 200 U/L penicillin at 37 °C 5% CO₂. For the *in vitro* experiments, both the drug tests and cytotoxicity assays, macrophages were cultured in RPMI-1640 supplemented with 20% FBS, 5% LCCM, and 200 U/L penicillin at 37 °C (5% CO₂).

Cytotoxicity assay. A Trypan Blue® assay was used to determine the toxicity of the products for BMDM and L929 fibroblasts. Cells were distributed in 24-well plates (4x10⁵ BMDMs/well or 5x10⁴ fibroblasts/well) and incubated with every product at increasing concentrations (1, 5, 20, 50, and 100 μM). Pentamidine isethionate was used at concentrations of 0.1, 0.2, 0.5, 1, 5, 10, and 20 μM, and meglumine antimoniate was used at concentrations of 50, 100, 300, 500, and 1000 μM. Control groups incubated with diluent (DMSO) or physiological saline solution were also included. After 72 h, cells were collected and incubated with Trypan Blue® (0.4%) in culture medium (1:1). After a few min, alive and dead cells were counted in hemocytometer and a survival ratio was established for every concentration by comparing them with control groups. Thus, the cytotoxic concentration of 50% (CC₅₀, the concentration that inhibits cell growth by 50%) was determined for every compound and reference drug. Assays were

performed in triplicate, and the results are expressed as the mean percentage reduction of viability of three independent experiments. CC₅₀ was determined using regression analysis.

Promastigotes *in vitro* assay. Cell viability was evaluated *in vitro* by cultivating 5×10⁶ *L. infantum* promastigotes in the presence of increasing concentrations of the given compound (1-100 μM for compounds **5**, **6** and **11**; 1-20 μM for compounds, vorinostat and pentamidine isethionate), including diluent (DMSO) controls and using pentamidine isethionate as a reference drug control. After 48 h, quantification of viable cells was assessed by measuring the cleavage of 3-(4,5-dimethylthiazol-2-yl)-2,5-diphenyl tetrazolium bromide (MTT) by metabolically active cells. Cells were incubated in 5 mg/mL MTT in PBS for 2 h at 24 °C. MTT cleavage was assessed with a multiwell spectrophotometer with a test wavelength of 595 nm and a reference wavelength of 690 nm. Assays were performed in triplicate, and the results are expressed as the mean percentage reduction of viability of three independent experiments. IC₅₀ was determined using regression analysis.

Intracellular amastigote *in vitro* assay. BMDMs were used as the infection model. BMDMs were counted and distributed (4×10^6 macrophages/well) in 24-well cell culture plates (GreinerBioOne) with round coverslips. Macrophages were left for a day to allow them to adhere to the coverslips. Then, they were infected with stationary-phase *L. infantum* promastigotes in a 10:1 parasite:macrophage ratio. Once infected, macrophages were incubated with each compound at increasing concentrations (0.2, 0.5, 0.8, 1, 5, 20, 50 and 100 μ M) for 48 h. Untreated controls and diluent controls (DMSO 0.5%) were included. Wells treated with pentamidine isethionate or meglumine antimoniate were included as reference drug controls and their IC₅₀ values were calculated as well. At least three independent experiments were performed.

In vitro results evaluation. Coverslips with macrophages were washed, fixed with methanol and stained with Giemsa. The percentage of infection was quantified with optical microscopy.

Macrophages were considered infected if they contained at least one amastigote. At least 3

independent experiments were performed for the evaluation of the intracellular amastigote assays. Every independent experiment included 3 wells with coverslips. In each coverslip, 10 random fields at 1000x magnification were examined, and a minimum of 200 macrophages per coverslip were counted. A regression analysis was performed to establish a dose-response relationship and to determine the inhibitory concentration 50% (IC₅₀). The concentration and infection level calculated from untreated wells were included as independent variables. The percentage of infection reduction was used as the dependent variable, and it was calculated as the difference between the average percentage of infection of control wells and the percentage of infection of treated wells, divided by the average percentage of infection of control wells corresponding to the experiment.

The selectivity index (SI) is defined as the ratio that measures the window between cytotoxicity and antiparasitic activity. It was calculated based on the formula SI = $CC_{50} \times (IC_{50})^{-1}$.

In vivo assays for biological evaluation.

Experimental infection. BALB/c mice were infected intraperitoneally with 10 million stationary-phase promastigotes in 200 μ L of 0.9% saline solution. Then, mice were divided into groups of 7 each.

Antileishmanial treatment. Each treated group received a daily maximum volume of 200 μ L of **5** previously vehiculized on nanoparticles (PLGA or gold nanoparticles). Doses of 10 mg/kg and 25 mg/kg were investigated. The treatment started 28 days after the infection date and lasted for 14 days. Mice were treated daily for 14 days intraperitoneally with 104 mg of Sb^V/kg (meglumine antimoniate) and were included as a reference control treatment. Mice that received free nanoparticles for 14 days were included as a control. Mice receiving only 0.9% saline solution were also included to rule out nanoparticle antileishmanial activity. Three independent experiments were performed with 7 mice per group.

Antileishmanial efficacy evaluation. Mice were sacrificed by cervical dislocation, and samples of spleen and liver were taken. Both organs were divided into three parts for evaluation of the

presence of *Leishmania* by microscopy, culture, and PCR. Liver and spleen imprints were made and then fixed in pure methanol and Giemsa-stained to detect amastigotes. Cultures were made with macerates of 20 mg of each organ using a combination of Evans' modified Tobie's medium (EMTM) solid phase prepared with rabbit blood and RPMI supplemented with 20% FBS and 5% human urine as the liquid phase. The cultures were kept for 3 months before being rejected as negative. *In vitro* subinoculations were performed weekly. The organ part was processed in a room exclusively intended for DNA extraction. DNA was obtained from the different weighed samples using the REAL DNA SSS Extraction Kit (RBME01). Each DNA extract was rehydrated in a final volume of 20 μ L of sterile water. To ensure that there was no contamination at this stage, extraction controls were carried out. These consisted of tubes of sterile water to which the whole extraction process was applied simultaneously with the biological samples. One control was used for every group of 7 biological samples. The extracted DNA was kept at -20 °C until amplification by PCR.

As a fully independent procedure for DNA extraction from biological samples taken from mice, DNA was also extracted from *L. infantum* promastigotes (MCAN/ES/2007/DP534) taken from cultures. The parasites were washed and counted with a hemocytometer and adjusted to a final concentration of 1000 parasites/ μ L to be used as a positive control in the PCR. Three negative controls were used: a) tube of PCR reagents without DNA, b) extraction controls, and c) DNA from uninfected mice.

Evaluation of parasite load in liver and spleen was performed by using a quantitative real-time PCR (qPCR) specific for *L. infantum*, adapted from a PCR-ELISA.⁸³ This qPCR is a TaqMan-based assay adjusted to be very sensitive and efficient for *L. infantum* DNA quantification, as previously reported.^{52,84} Each sample was analyzed in triplicate in a final reaction volume of 25 μL. The parasite load was obtained by interpolating the threshold cycle (Ct) values obtained for each biological sample in a previously constructed calibration curve. This calibration curve was made with serial dilutions of a *L. infantum* promastigote suspension of known cell density. The

final parasite load in the sample was expressed in terms of number of parasites/milligram of liver or spleen and was calculated from the values returned in the three replicates taking an adjusted average. Once the parasite load was quantified, the percentage of reduction in parasite load was calculated by comparing the parasite load of mice treated with the parasite load of untreated mice (animals receiving free nanoparticles).

Toxicity evaluation. For the in vivo acute toxicity evaluation, a group of 10 Swiss healthy mice was treated with a single dose of 500 mg/kg of 5 supported in gold nanoparticles. They were observed and sacrificed after 28 days. For the in vivo subacute toxicity evaluation, 25 mg/kg, 50 mg/kg, and 200 mg/kg doses were tested. Groups of healthy Swiss mice were treated for 14 days and sacrificed 28 days after the start of the experiment. Animals were weighed before the start of the experiment (before infection), before the start of the treatment, and weekly until the end of the experiment. They were also investigated for signs such as stress, pain, cutaneous signs, or diarrhea. After the sacrifice, the spleen and liver were weighed to look for splenomegaly or hepatomegaly, respectively. Blood samples were taken to carry out biochemical functional tests. Urea, creatinine, alkaline phosphatase, and transaminase plasma level tests were carried out using commercially available kits (Spinreact, Spain). In addition, structural integrity research was performed. Histological slides were obtained from kidney, spleen, and liver, stained with hematoxylin-eosin and fixed in paraffin. These preparations were investigated under light microscopy to find tissue damage after treatment. Thus, histopathological signs were searched for in the liver (steatosis, vesicles, necrosis foci, edema), kidney (glomeruli and tubular abnormalities), and spleen (abnormalities in the follicles and the splenic structure). Other less specific signs were also evaluated, such as the infiltration of inflammatory cells in these tissues. These procedures were also carried out on the infected treated and untreated mice from the effectiveness experiments to confirm the absence of toxicity on infected mice.

Statistical analysis. In order to evaluate the *in vivo* effectiveness results, non-parametric Mann-Whitney's test was performed while ANOVA test was used for analyzing toxicity data. Statistical software SPSS 20.0 was used. Regression analysis was performed in order to establish a dose-response relationship and to determinate the IC_{50} and CC_{50} values.

Cardiotoxicity study on HEK-293 hERG cells. Assay Protocol.

The FluxOR™ potassium channel assay was performed as outlined in the Invitrogen information sheet and performed on the FLIPR TETRA (Molecular Devices). Powerload™ concentrate and water-soluble probenecid were used as directed by the kit to enhance the dye solubility and retention, respectively, and were added in the first step. Then, FluxOR™ was added and mixed with powerload and probenecid. FluxOR™ loading buffer was 165 mM NaCl, 4.5 mM KCl, 2 mM CaCl₂, 1mM MgCl, 10 mM Hepes and 10 mM glucosa. The buffer pH was adjusted to 7.4. Media were removed from the cell plates manually, and 80 µL of loading buffer containing the FluxOR™ dye mix was applied to each. The dye was loaded for 60 min at r.t. and then removed manually. The cell plates were subsequently washed once with assay buffer before adding the compounds in assay buffer, with Biomek, to a final volume of 100 μL. The plates were incubated at r.t. (23-25 °C) for 30 min to allow equilibration of the test compounds. Stimulation buffer (Tl₂SO₄ + K₂SO₄) was prepared following the manufacturer's instructions. The injection of stimulation buffer into the plates was performed on FLIPR TETRA to analyze the kinetics from t0, when the stimulation buffer was added, to 120 seconds. The controls and 5 were prepared in DMSO (10 points, 1:2 dilutions) and added to cell plates at a 1:200 dilution (2 μL of compound/400μL of buffer) using a Biomek unit (Beckman Coulter). The DMSO concentration was 0.5% in all cases. Compound 5 was tested at the highest concentration of 125 μ M and all experiments conducted in triplicate. Positive control (1 μ M astemizole) and negative control (0.5% DMSO) were introduced in each plate. IC₅₀ values were calculated. HEK-293 hERG cells were used at P17.

Compound **5** displayed an IC₅₀ of 96.22 μ M (control IC₅₀: astemizole 2.6 \pm 0.1; bepridil 1.4 \pm 0.2; haloperidol 1.16 \pm 0.3; terfenadine 1.2 \pm 0.2).

Cytochrome P450 inhibitory evaluation of compound 5

Incubations for evaluating CYP inhibition were conducted in a 96-well plate format at 37 °C. The final incubation (200 μL total volume) contained 0.25 mg/mL of human liver microsome (HLM) protein in 100 mM potassium phosphate buffer (pH 7.4), 1 mM NADPH, and test compound 5 at 0.078, 0.313, 0.625, 1.25, 2.5, 5, 11, 22, 44 and 88 μM. The probe reaction for CYP3A4 was conducted with 50 μM testosterone and HLM protein for 15 min. In the case of the CYP2D6 probe, the reaction was conducted with 22 μM dextromethorphan for 30 min. The CYP2C9 probe reaction was conducted with 10 μM diclofenac for 45 min. Incubations were carried out in the linear time range and at substrate concentrations close to their respective values of Michaelis-Menten constant. Reactions were monitored using liquid chromatography coupled to tandem mass spectrometry (LC-MS/MS). Control inhibitors, such as ketoconazole for CYP3A4, quinidine for CYP2D6, or sulfaphenazole for CYP2C9, were included in all incubation plates.

To reduce the DMSO content to below 1% in the enzyme incubations as commonly practiced, test compound **5** was dissolved in DMSO–ACN (35:65) (v/v) and further 1/2 serially diluted to provide 10 concentration levels. Then, test compound **5** in DMSO/ACN (35:65) (v/v) (2 μ L) was combined with 98 μ L of NADPH solution, and the reactions were initiated by the addition of 100 μ L of enzyme-substrate solution. Reactions were terminated with the addition of a quenching solution (90 μ L) of ACN containing internal standards for LC-MS/MS analysis (60 ppb cortisone, 100 ppb 4'-hydroxydiclofenac 13C6, 60 ppb levallorphan).

Robust Z' factor was determined for assay quality control purposes, and it was established in 0.825 for CYP3A4, 0.924 for CYP2D6 and 0.806 for CYP2C9. Additionally, the IC₅₀ values for the control inhibitors were in good agreement with the results obtained in related studies.

Compound 5 metabolic stability evaluation in human liver microsomes

Total incubation volume: 400 μ L. Protein concentration: 1 mg/mL. NADPH: 1.3 mM. A stock solution of **5** was prepared in DMSO at 10 mM. The final concentration of **5** in the assay was 1 μ M. A stock solution of 2.66 mM NADPH was prepared by dissolving the appropriate amount of NADPH in 100 mM potassium phosphate buffer.

The reaction was initiated by adding a human liver microsome (HLM) solution (1 mg/mL) to an equal volume of buffer solution containing test compound and cofactors at the proper concentrations. Reactions without NADPH were also incubated to rule out non-NADPH metabolism or chemical instability in the incubation buffer. One positive control (verapamil) was included to monitor the incubation course. All reactions were terminated using 50 μ L of ice-cold ACN at 0, 5, 15, 30, 45, and 60 min. The plates were centrifuged at 3500 rpm for 15 min. All experiments were conducted in triplicate.

Samples were monitored for parent compound disappearance by LC-MS in Multiple Reaction Monitoring (MRM) mode using a previously developed quantitation method for compound 5. Key instrumental and analytical conditions are shown in the Supporting Information. The peak area of the analyte was used to calculate the percentage of remaining compound at each incubation time. The natural logarithm of the percentage of remaining parent compound was plotted versus incubation time to calculate the half-life using the following equation:

Half-life $(t_{1/2})$ (min) = 0.693/k

[k: The slope of the natural log of the percent remaining versus time].

Intrinsic hepatic clearance (CL_{int H}) can be determined by the following equation:

 $CL_{int H} = [(Ln 2)/t_{1/2}] * [volume incubation (mL)/microsomal protein (mg)] * 45 (MPPGL) * [1500] g human liver/70 Kg human body weight]$

Units for CL_{int H} are usually expressed as mL/min/mg microsomal protein. MPPGL = Referred to as mg microsomal protein per gram liver.

The percentages of remaining parent compound for verapamil and **5** are reported in the Supporting Information (Table 2 and Table 3, respectively). The positive control (verapamil)

shows a half-life value consistent with the validation and published results (see Table 4, Figure 1, and Figure 2 in the Supporting Information). Analysis of the percentage of compound 5 remaining in the minus NADPH cofactor incubations did not show the metabolism of the parent from nondependent NADPH enzymes (see Table 3 and Figure 2, Supporting Information).

Compound **5** displays a half-life value equal to 6.10 min (see Table 4, Supporting Information). The predicted intrinsic clearance calculated for compound **5** was established as 113.06 µL/min/mg protein (see Table 4, Supporting Information).

Compound 5 metabolite profiling and identification

The *in vitro* profiling and identification of main potential metabolites from compound **5** in HLM incubations was conducted by liquid chromatography coupled to high-resolution mass spectrometry (LC-HRMS). The same **5** incubations in HLM at six incubation times (0, 5, 15, 30, 45 and 60 min) prepared for the metabolic stability study were considered for this investigation. Six main metabolites from **5** have been found. Detailed information can be found in the Supporting Information (Table 5, Table 6, and Figure 3).

Ames test

Two mutant strains, *S. typhimurium* TA98 and *S. typhimurium* TA100, were used to detect frameshift and base-pair mutations, respectively. The bacteria were maintained frozen and stored in total darkness until used. Both bacteria were inoculated in nutrient broth and incubated at 37 °C for 20 h prior to the test. The following chemicals were purchased from EBPI: Davis-Mingioli salt (5.5 times concentrated), D-glucose (40%, w/v), bromocresol purple (2 mg/mL), D-biotin (0.1 mg/mL), and L-histidine (0.1 mg/mL). Two sterile standard mutagens were sodium azide (NaN₃, 0.5 μ g/100 μ L) for *S. typhimurium* TA100 and 2-nitrofluorene (2-NF, 30 μ g/100 μ L) for *S. typhimurium* TA98. All chemicals were kept at 3 ± 1 °C until use. Reagent mixture: Davis-Mingioli salt (21.62 mL), D-glucose (4.75 mL), bromocresol purple (2.38 mL), D biotin (1.19 mL) and L-histidine (0.06 ml) were mixed aseptically in a sterile bottle. Compound

 ${f 5}$ was stored at 4 °C and kept in total darkness until used. This substance was dissolved in DMSO and filtered through a 0.22 μm membrane filter. Then, three sample dilutions of the compound were prepared by making up the quantity to be tested with sterilized distilled water to achieve the appropriate dilution.

A commercial test kit, the Muta-ChromoPlateTM, from Environmental Bio-detection Products Inc. (EBPI, Ontario, Canada) was used to evaluate the mutagenicity of **5**. This test kit is based on the "Ames Test", ⁶⁷ and on an assay performed entirely in liquid culture, which is the "fluctuation test". ^{85,86} Suspensions of bacterial cells were exposed to 3 different concentrations of **5** in 96-well flat-bottomed plates, as well as a positive and negative control for reverting growth and scoring. After 5 days of incubation, reverting colonies were detected by the change of color from blue to yellow on the solvent control plates. The results were also taken through days 3-7 for better interpretation. All yellow, partially yellow or turbid wells were scored as positive, while all purple wells were scored as negative. The number of positive wells for each plate was recorded, and their number was counted and compared to that of spontaneous reverting colonies. The "background" (i.e., no test material added) plate was used as a reference for the level of spontaneous or background mutation of the assay organism.

For a sample dilution to be mutagenic, the number of positive wells had to be significantly higher than the number of positive wells in the "background" plate (spontaneous mutation), and this was determined statistically.⁸⁷ Additionally, according to the manufacturer table, the level of mutagenicity was classified as strongly mutagenic if p < 0.001, moderately mutagenic if p < 0.01 and mildly mutagenic if p < 0.05.

Computational Methodology

Homology modeling: LiHDAC-I of *L. infantum* was built in a tridimensional (3D) structure using the protein sequence retrieved from the UniProt database, code: A4HZ67. Further, the I-TASSER server⁷³ was used to build the 3D structure of the protein under homology modeling and multiple-threading procedures. The following PDB IDs were used as starting points for the

modeling: 4A69, 4BKX and 4LY1. The Zn coordinates located at the catalytic site in LiHDAC-I were added from the zinc-binding domain in the crystal structures used as templates for each model, as described elsewhere.88 Then, 3D models were submitted to the ModRefiner Server (https://zhanglab.ccmb.med.umich.edu/ModRefiner/), to perform structure refinement and improve the local and global quality.89 The quality of the models was structurally evaluated by the Ramachandran plot from Procheck (https://www.ebi.ac.uk/thorntonsrv/software/PROCHECK/).90 Other protein structural properties were measured for structure validation, such (http://servicesn.mbi.ucla.edu/ERRAT/),⁹¹ Errat Prosa (https://prosa.services.came.sbg.ac.at/prosa.php),92 and MolProbity (http://molprobity.biochem.duke.edu).93 The crystal structure of LiSIR2rp1 was retrieved from Protein Data Bank (PDB), PDB code: 5OLO.74 Water molecules were removed, and the 3D structure was further used for docking studies.

Docking simulations: The synthesized compounds were docked on LiHDAC-I and LiSIR2rp1 models using AutoDock Vina⁹⁴ on a Linux platform under a blind docking protocol. The 3D models of parasitic LiHDAC-I and LiSIR2rp1 (5OLO⁷⁴) were validated with a blind docking using vorinostat and nicotinamide for the LiHDAC-I and LiSIR2rp1 models, respectively. Polar hydrogen atoms were added to the proteins, and the protein Kollman charges were calculated using AutodockTools 1.5.6.⁹⁵ Ligands were drawn in Gaussian View 3.0⁹⁶ and geometrically optimized using Gaussian 09⁹⁷ at the AM1 semiempirical level. The output files were converted to PDB file format using Molekel 4.3 software.⁹⁸ Only polar hydrogen atoms were conserved, and the partial atomic charge of the ligands was calculated using AutodockTools 1.5.6⁹⁵ with the Gasteiger-Marsili formalism.⁹⁹ Blind docking was performed using a 126 ų point grid with 0.375 ų grid spacing centered on the protein. The interactions of the ligands with the proteins were visualized using AutoDock Tools 1.5.6,⁹⁵ and figures were created using Chimera UCSF 1.10.1¹⁰⁰ and Pymol V 2.0.¹⁰¹

Ethical statement. All experiments were performed in accordance with the EU Directive 2010/63/EU and the recommendations of the Federation for Laboratory Animals Science Associations (FELASA). The experiments were approved by the Ethics Committee of Animal Experimentation (CEEA) of the University of Granada (CEEA 455–2013).

Acknowledgments

We acknowledge financial support to SPF from the Junta de Andalucía (Spain). This research was supported by the project P06-CTS-01407 from the Junta de Andalucía (Spain), the project GREIB.PT-2010-10 from the Universidad de Granada (Spain), and the project 20F12/7 from the Universidad de Granada (Spain). The authors wish to thank Dr. Montserrat Gállego (University of Barcelona) for kindly donating the *L. major* and *L. donovani* strains, and Dr. Francine Pratlong (University of Montpellier) for kindly donating the *L. tropica* strain used in this work. JCB and YSL thank to grants from CONACYT CB-254600, CONACYT-APN-782, Proyectos Insignia IPN-2015, SIP-COFAA/IPN, México.

Supporting Information

The Supporting Information is available free of charge on the ACS Publications website at DOI: Experimental procedures for compounds **10** and **11**. Tables and Figures indicated throughout the manuscript as Supporting Information. LC-MS conditions for the metabolic stability evaluation in human liver microsomes, and electrophoretic mobility measurements. Molecular Formula Strings including biological data is also available.

PDB codes for LiHDAC bound to compounds **5** (LiHDAC_5), **10** (LiHDAC_10), **11** (LiHDAC_11), and vorinostat (LiHDAC_vorinostat). PDB codes for Lisir2rp1 bound to compounds **5** (Lisir2rp1_5), **6** (Lisir2rp1_6), **10** (Lisir2rp1_10), **11** (Lisir2rp1_11), nicotinamide (Lisir2rp1_NCA), and vorinostat (Lisir2rp1_vorinostat). Authors will release the atomic coordinates and experimental data upon article publication.

Author information

Corresponding Author

*For J.A. G-V: phone, (34) 958 240719; E-mail, jagvidal@ugr.es

Author Contributions

M.T.C. and V.C.L. contributed equally.

Notes

The authors declare no competing financial interest.

References

- (1) Alvar, J.; Vélez, I. D.; Bern, C.; Herrero, M.; Desjeux, P.; Cano, J.; Jannin, J.; den Boer, M.; the WHO Leishmaniasis Control Team. Leishmaniasis Worldwide and Global Estimates of Its Incidence. *PLoS One* **2012**, *7*, e35671.
- (2) World Health Organization. Leishmaniasis. https://www.who.int/news-room/fact-sheets/detail/leishmaniasis (accessed February 27, 2020).
- (3) Martin-Sanchez, J.; Gramiccia, M.; Di Muccio, T.; Ludovisi, A.; Morillas-Márquez, F. Isoenzymatic Polymorphism of *Leishmania infantum* in Southern Spain. *Trans. R. Soc. Trop. Med. Hyg.* **2004**, *98*, 228–232.
- (4) Aliaga, L.; Cobo, F.; Mediavilla, J. D.; Bravo, J.; Osuna, A.; Amador, J. M.; Martín-Sánchez, J.; Cordero, E.; Navarro, J. M. Localized Mucosal Leishmaniasis Due to *Leishmania* (*Leishmania*) *infantum*: Clinical and Microbiologic Findings in 31 Patients. *Medicine* 2003, 82, 147–158.
- (5) Martín-Sánchez, J.; Morales-Yuste, M.; Acedo-Sánchez, C.; Barón, S.; Díaz, V.; Morillas-Márquez, F. Canine Leishmaniasis in Southeastern Spain. *Emerg. Infect. Dis.* 2009, 15, 795–798.
- (6) Alves, F.; Bilbe, G.; Blesson, S.; Goyal, V.; Monnerat, S.; Mowbray, C.; Ouattara, G. M.; Pécoul, B.; Rijal, S.; Rode, J.; Solomos, A.; Strub-Wourgaft, N.; Wasunna, M.; Wells, S.; Zijlstra, E. E.; Arana, B.: Alvar, J. Recent Development of Visceral Leishmaniasis

- Treatments: Successes, Pitfalls, and Perspectives. *Clin. Microbiol. Rev.* **2018**, *31*, e00048-18.
- (7) Sundar, S.; Olliaro, P. L. Miltefosine in the Treatment of Leishmaniasis: Clinical Evidence for Informed Clinical Risk Management. *Ther. Clin. Risk Manag.* **2007**, *3*, 733–740.
- (8) Rybniker, J.; Goede, V.; Mertens, J.; Ortmann, M.; Kulas, W.; Kochanek, M.; Benzing, T.; Arribas, J. R.; Fätkenheuer, G. Treatment of Visceral Leishmaniasis with Intravenous Pentamidine and Oral Fluconazole in an HIV-Positive Patient with Chronic Renal Failure

 a Case Report and Brief Review of the Literature. *Int. J. Infect. Dis.* **2010**, *14*, e522–e525.
- (9) Peña, I.; Pilar Manzano, M.; Cantizani, J.; Kessler, A.; Alonso-Padilla, J.; Bardera, A. I.; Alvarez, E.; Colmenarejo, G.; Cotillo, I.; Roquero, I.; de Dios-Anton, F.; Barroso, V.; Rodriguez, A.; Gray, D. W.; Navarro, M.; Kumar, V.; Sherstnev, A.; Drewry, D. H.; Brown, J. R.; Fiandor, J. M.; Martin, J. J. New Compound Sets Identified from High Throughput Phenotypic Screening Against Three Kinetoplastid Parasites: An Open Resource. Sci. Rep. 2015, 5, 8771.
- (10) Ruberto, I.; Szoor, B.; Clark, R.; Matthews, K. R. Investigating Mammalian Tyrosine Phosphatase Inhibitors as Potential 'Piggyback' Leads to Target *Trypanosoma brucei* Transmission. *Chem. Biol. Drug Des.* 2013, 81, 291–301.
- (11) Ojo, K. K.; Arakaki, T. L.; Napuli, A. J.; Inampudi, K. K.; Keyloun, K. R.; Zhang, L.; Hol, W. G. J.; Verlinde, C. L. M. J.; Merritt, E. A.; Van Voorhis, W. C. Structure Determination of Glycogen Synthase Kinase-3 from *Leishmania major* and Comparative Inhibitor Structure–Activity Relationships with *Trypanosoma brucei* GSK-3. *Mol. Biochem. Parasitol.* 2011, 176, 98–108.
- (12) Falkenberg, K. J.; Johnstone, R. W. Histone Deacetylases and Their Inhibitors in Cancer, Neurological Diseases and Immune Disorders. *Nat. Rev. Drug Discov.* **2014**, *13*, 673–691.

- (13) Sumanadasa, S. D. M.; Goodman, C. D.; Lucke, A. J.; Skinner-Adams, T.; Sahama, I.; Haque, A.; Do, T. A.; McFadden, G. I.; Fairlie, D. P.; Andrews, K. T. Antimalarial Activity of the Anticancer Histone Deacetylase Inhibitor SB939. *Antimicrob. Agents Chemother.* 2012, 56, 3849–3856.
- (14) Andrews, K. T.; Haque, A.; Jones, M. K. HDAC Inhibitors in Parasitic Diseases. *Immunol. Cell Biol.* **2012**, *90*, 66–77.
- (15) Paris, M.; Porcelloni, M.; Binaschi, M.; Fattori, D. Histone Deacetylase Inhibitors: From Bench to Clinic. *J. Med. Chem.* **2008**, *51*, 1505–1529.
- (16) Grant, S.; Easley, C.; Kirkpatrick, P. Vorinostat. Nat. Rev. Drug Discov. 2007, 6, 21–22.
- (17) Herman, D.; Jenssen, K.; Burnett, R.; Soragni, E.; Perlman, S. L.; Gottesfeld, J. M. Histone Deacetylase Inhibitors Reverse Gene Silencing in Friedreich's Ataxia. *Nat. Chem. Biol.* 2006, 2, 551–558.
- (18) Giannini, G.; Battistuzzi, G.; Vignola, D. Hydroxamic Acid Based Histone Deacetylase Inhibitors with Confirmed Activity against the Malaria Parasite. *Bioorg. Med. Chem. Lett.* 2015, 25, 459–461.
- (19) Mai, A.; Cerbara, I.; Valente, S.; Massa, S.; Walker, L. A.; Tekwani, B. L. Antimalarial and Antileishmanial Activities of Aroyl-Pyrrolyl-Hydroxyamides, a New Class of Histone Deacetylase Inhibitors. *Antimicrob. Agents Chemother.* **2004**, *48*, 1435–1436.
- (20) Guerrant, W.; Mwakwari, S. C.; Chen, P. C.; Khan, S. I.; Tekwani, B. L.; Oyelere, A. K. A Structure–Activity Relationship Study of the Antimalarial and Antileishmanial Activities of Nonpeptide Macrocyclic Histone Deacetylase Inhibitors. *ChemMedChem* 2010, 5, 1232–1235.
- (21) Sodji, Q.; Patil, V.; Jain, S.; Kornacki, J. R.; Mrksich, M.; Tekwani, B. L.; Oyelere, A. K. The Antileishmanial Activity of Isoforms 6- and 8-Selective Histone Deacetylase Inhibitors. *Bioorg. Med. Chem. Lett.* **2014**, *24*, 4826–4830.

- (22) Patil, V.; Guerrant, W.; Chen, P. C.; Gryder, B.; Benicewicz, D. B.; Khan, S. I.; Tekwani, B. L.; Oyelere, A. K. Antimalarial and Antileishmanial Activities of Histone Deacetylase Inhibitors with Triazole-Linked Cap Group. *Bioorg. Med. Chem.* 2010, 18, 415–425.
- (23) McGaughey, G. B.; Gagné, M.; Rappé, A. K. π-Stacking Interactions Alive and Well in Proteins. *J. Biol. Chem.* **1998**, *273*, 15458–15463.
- (24) Ho, C. Y.; Strobel, E.; Ralbovsky, J.; Galemmo, R. A. Improved Solution- and Solid-Phase Preparation of Hydroxamic Acids from Esters. *J. Org. Chem.* **2005**, *70*, 4873–4875.
- (25) Ech-Chahad, A.; Minassi, A.; Berton, L.; Appendino, G. An Expeditious Hydroxyamidation of Carboxylic Acids. *Tetrahedron Lett.* **2005**, *46*, 5113–5115.
- (26) Giacomelli, G.; Porcheddu, A.; Salaris, M. Simple One-Flask Method for the Preparation of Hydroxamic Acids. *Org. Lett.* **2003**, *5*, 2715–2717.
- (27) Terracciano, S.; Micco, S. D.; Bifulco, G.; Gallinari, P.; Riccio, R.; Bruno, I. Synthesis and Biological Activity of Cyclotetrapeptide Analogues of the Natural HDAC Inhibitor FR235222. *Bioorg. Med. Chem.* **2010**, *18*, 3252–3260.
- (28) Guerrant, W.; Patil, V.; Canzoneri, J. C.; Oyelere, A. K. Dual Targeting of Histone Deacetylase and Topoisomerase II with Novel Bifunctional Inhibitors. *J. Med. Chem.* **2012**, *55*, 1465–1477.
- (29) Marek, L.; Hamacher, A.; Hansen, F. K.; Kuna, K.; Gohlke, H.; Kassack, M. U.; Kurz, T. Histone Deacetylase (HDAC) Inhibitors with a Novel Connecting Unit Linker Region Reveal a Selectivity Profile for HDAC4 and HDAC5 with Improved Activity against Chemoresistant Cancer Cells. *J. Med. Chem.* **2013**, *56*, 427–436.
- (30) Daniel, K. B.; Sullivan, E. D.; Chen, Y.; Chan, J. C.; Jennings, P. A.; Fierke, C. A.; Cohen, S.
 M. Dual-Mode HDAC Prodrug for Covalent Modification and Subsequent Inhibitor
 Release. J. Med. Chem. 2015, 58, 4812–4821.

- (31) Mai, A.; Esposito, M.; Sbardella, G.; Massa, S. A New Facile and Expeditious Synthesis of N-Hydroxy-N'-Phenyloctanediamjde, a Potent Inducer of Terminal Cytodifferecntiation. Org. Prep. Proced. Int. 2001, 33, 391–394.
- (32) Carpino, L. A.; El-Faham, A.; Albericio, F. Efficiency in Peptide Coupling: 1-Hydroxy-7-Azabenzotriazole vs 3,4-Dihydro-3-Hydroxy-4-Oxo-1,2,3-Benzotriazine. *J. Org. Chem.* **1995**, *60*, 3561–3564.
- (33) Saxena, A.; Lahav, T.; Holland, N.; Aggarwal, G.; Anupama, A.; Huang, Y.; Volpin, H.; Myler, P. J.; Zilberstein, D. Analysis of the *Leishmania donovani* Transcriptome Reveals an Ordered Progression of Transient and Permanent Changes in Gene Expression during Differentiation. *Mol. Biochem. Parasitol.* 2007, 152, 53–65.
- (34) Alcolea, P. J.; Alonso, A.; Gómez, M. J.; Moreno, I.; Domínguez, M.; Parro, V.; Larraga, V. Transcriptomics throughout the Life Cycle of *Leishmania infantum*: High down-Regulation Rate in the Amastigote Stage. *Int. J. Parasitol.* **2010**, *40*, 1497–1516.
- (35) Pontiki, E.; Hadjipavlou-Litina, D. Histone Deacetylase Inhibitors (HDACIs). Structure—
 Activity Relationships: History and New QSAR Perspectives. *Med. Res. Rev.* **2012**, *32*, 1–
 165.
- (36) Rajak, H.; Singh, A.; Raghuwanshi, K.; Kumar, R.; Dewangan, P. K.; Veerasamy, R.; Sharma, P. C.; Dixit, A.; Mishra, P. A Structural Insight into Hydroxamic Acid Based Histone Deacetylase Inhibitors for the Presence of Anticancer Activity. *Curr. Med. Chem.* 2014, 21, 2642–2664.
- (37) Zwick, V.; Nurisso, A.; Simões-Pires, C.; Bouchet, S.; Martinet, N.; Lehotzky, A.; Ovadi, J.; Cuendet, M.; Blanquart, C.; Bertrand, P. Cross Metathesis with Hydroxamate and Benzamide BOC-Protected Alkenes to Access HDAC Inhibitors and Their Biological Evaluation Highlighted Intrinsic Activity of BOC-Protected Dihydroxamates. *Bioorg. Med. Chem. Lett.* 2016, 26, 154–159.

- (38) Wuts, P. G. M.; Greene, T. W. *Greene's Protective Groups in Organic Synthesis*; John Wiley & Sons, Inc.: Hoboken, NJ, 2007; pp 106-116 and pp 152-156.
- (39) Mourtas, S.; Gatos, D.; Karavoltsos, M.; Katakalou, C.; Barlos, K. Resin-Bound Mercapto Acids: Synthesis and Application. *Tetrahedron Lett.* **2002**, *43*, 3419–3421.
- (40) Gaffney, P. R. J.; Changsheng, L.; Rao, M. V.; Reese, C. B.; Ward, J. G. Some Substituted 9-Phenylxanthen-9-yl Protecting Groups. *J. Chem. Soc. Perkin* 1 **1991**, 1355–1360.
- (41) Reissmann, S.; Steinmetzer, T.; Greiner, G.; Seyfarth, L.; Besser, D.; Schumann, C. 2.6 Other Side-Chain Protections (III). 2.6.4 Hydroxy Group. In *Houben-Weyl Methods of Organic Chemistry Vol. E 22a, 4th Edition Supplement*; Goodman, M. Ed.; Georg Thieme Verlag: Stuttgart, 2004; p 369.
- (42) Neal, R. A.; Allen, S.; McCoy, N.; Olliaro, P.; Croft, S. L. The Sensitivity of *Leishmania* Species to Aminosidine. *J. Antimicrob. Chemother.* **1995**, *35*, 577–584.
- (43) Escobar, P.; Matu, S.; Marques, C.; Croft, S. L. Sensitivities of *Leishmania* Species to Hexadecylphosphocholine (Miltefosine), ET-18-OCH₃ (Edelfosine) and Amphotericin B. *Acta Trop.* **2002**, *81*, 151–157.
- (44) Don, R.; Ioset, J.-R. Screening Strategies to Identify New Chemical Diversity for Drug Development to Treat Kinetoplastid Infections. *Parasitology* **2014**, *141*, 140–146.
- (45) Corpas-López, V.; Díaz-Gavilán, M.; Franco-Montalbán, F.; Merino-Espinosa, G.; López-Viota, M.; López-Viota, J.; Belmonte-Reche, E.; Pérez-del Palacio, J.; de Pedro, N.; Gómez-Vidal, J. A.; Morillas-Márquez, F.; Martín-Sánchez, J. A Nanodelivered Vorinostat Derivative Is a Promising Oral Compound for the Treatment of Visceral Leishmaniasis. *Pharmacol. Res.* 2019, 139, 375–383.
- (46) Das, S.; Roy, P.; Mondal, S.; Bera, T.; Mukherjee, A. One Pot Synthesis of Gold Nanoparticles and Application in Chemotherapy of Wild and Resistant Type Visceral Leishmaniasis. *Colloids Surf. B Biointerfaces* **2013**, *107*, 27–34.

- (47) Santos, D. M.; Carneiro, M. W.; de Moura, T. R.; Soto, M.; Luz, N. F.; Prates, D. B.; Irache, J. M.; Brodskyn, C.; Barral, A.; Barral-Netto, M.; Espuelas, S.; Borges, V. M.; de Oliveira, C.
 I. PLGA Nanoparticles Loaded with KMP-11 Stimulate Innate Immunity and Induce the Killing of *Leishmania*. *Nanomedicine Nanotechnol*. *Biol. Med.* 2013, 9, 985–995.
- (48) Venier-Julienne, M. C.; Vouldoukis, I.; Monjour, L.; Benoit, J. P. In Vitro Study of the Anti-Leishmanial Activity of Biodegradable Nanoparticles. *J. Drug Target.* **1995**, *3*, 23–29.
- (49) Frézard, F.; Demicheli, C.; Ribeiro, R. R. Pentavalent Antimonials: New Perspectives for Old Drugs. *Molecules* 2009, 14, 2317–2336.
- (50) Bretagne, S.; Durand, R.; Olivi, M.; Garin, J. F.; Sulahian, A.; Rivollet, D.; Vidaud, M.; Deniau, M. Real-Time PCR as a New Tool for Quantifying *Leishmania infantum* in Liver in Infected Mice. *Clin. Diagn. Lab. Immunol.* **2001**, *8*, 828–831.
- (51) Moreira, N. das D.; Vitoriano-Souza, J.; Roatt, B. M.; Vieira, P. M. de A.; Ker, H. G.; de Oliveira Cardoso, J. M.; Giunchetti, R. C.; Carneiro, C. M.; de Lana, M.; Reis, A. B. Parasite Burden in Hamsters Infected with Two Different Strains of *Leishmania* (*Leishmania*) infantum: "Leishman Donovan Units" versus Real-Time PCR. PLoS One 2012, 7, e47907.
- (52) Corpas-López, V.; Morillas-Márquez, F.; Navarro-Moll, M. C.; Merino-Espinosa, G.; Díaz-Sáez, V.; Martín-Sánchez, J. (–)-α-Bisabolol, a Promising Oral Compound for the Treatment of Visceral Leishmaniasis. J. Nat. Prod. 2015, 78, 1202–1207.
- (53) Borborema, S. E. T.; Osso Junior, J. A.; de Andrade Junior, H. F.; do Nascimento, N. Biodistribution of Meglumine Antimoniate in Healthy and *Leishmania* (*Leishmania*) infantum chagasi-Infected BALB/c Mice. Mem. Inst. Oswaldo Cruz 2013, 108, 623-630.
- (54) Gangneux, J.-P.; Dullin, M.; Sulahian, A.; Garin, Y. J.-F.; Derouin, F. Experimental Evaluation of Second-Line Oral Treatments of Visceral Leishmaniasis Caused by *Leishmania infantum. Antimicrob. Agents Chemother.* **1999**, *43*, 172–174.
- (55) van Griensven, J.; Boelaert, M. Combination Therapy for Visceral Leishmaniasis. *The Lancet* **2011**, *377*, 443–444.

- (56) Tavares, J.; Ouaissi, A.; Kong Thoo Lin, P.; Loureiro, I.; Kaur, S.; Roy, N.; Cordeiro-da-Silva, A. Bisnaphthalimidopropyl Derivatives as Inhibitors of *Leishmania* SIR2 Related Protein 1.
 ChemMedChem 2010, 5, 140–147.
- (57) Tavares, J.; Ouaissi, A.; Silva, A. M.; Lin, P. K. T.; Roy, N.; Cordeiro-da-Silva, A. Anti-Leishmanial Activity of the Bisnaphthalimidopropyl Derivatives. *Parasitol. Int.* **2012**, *61*, 360–363.
- (58) Li, A. P. Screening for Human ADME/Tox Drug Properties in Drug Discovery. *Drug Discov. Today* **2001**, *6*, 357–366.
- (59) Obach, R. S. Prediction of Human Clearance of Twenty-Nine Drugs from Hepatic Microsomal Intrinsic Clearance Data: An Examination of In Vitro Half-Life Approach and Nonspecific Binding to Microsomes. *Drug Metab. Dispos.* 1999, 27, 1350–1359.
- (60) Brian Houston, J. Utility of in Vitro Drug Metabolism Data in Predicting in Vivo Metabolic Clearance. *Biochem. Pharmacol.* **1994**, *47*, 1469–1479.
- (61) Kadam, R. S.; Bourne, D. W. A.; Kompella, U. B. Nano-Advantage in Enhanced Drug Delivery with Biodegradable Nanoparticles: Contribution of Reduced Clearance. *Drug Metab. Dispos.* 2012, 40, 1380–1388.
- (62) Obach, R. S.; Walsky, R. L.; Venkatakrishnan, K.; Gaman, E. A.; Houston, J. B.; Tremaine, L. M. The Utility of *in Vitro* Cytochrome P450 Inhibition Data in the Prediction of Drug-Drug Interactions. *J. Pharmacol. Exp. Ther.* 2006, 316, 336–348.
- (63) Pollard, C. E.; Gerges, N. A.; Bridgland-Taylor, M. H.; Easter, A.; Hammond, T. G.; Valentin, J.-P. An Introduction to QT Interval Prolongation and Non-Clinical Approaches to Assessing and Reducing Risk. *Br. J. Pharmacol.* 2010, 159, 12–21.
- (64) Pollard, C. E.; Skinner, M.; Lazic, S. E.; Prior, H. M.; Conlon, K. M.; Valentin, J.-P.; Dota, C. An Analysis of the Relationship Between Preclinical and Clinical QT Interval-Related Data.
 Toxicol. Sci. 2017, 159, 94–101.

- (65) Yao, X.; Anderson, D. L.; Ross, S. A.; Lang, D. G.; Desai, B. Z.; Cooper, D. C.; Wheelan, P.; McIntyre, M. S.; Bergquist, M. L.; MacKenzie, K. I.; Becherer, J. D.; Hashim, M. A. Predicting QT Prolongation in Humans during Early Drug Development Using HERG Inhibition and an Anaesthetized Guinea-Pig Model. *Br. J. Pharmacol.* 2008, 154, 1446–1456.
- (66) Kuryshev, Y. A.; Wang, L.; Wible, B. A.; Wan, X.; Ficker, E. Antimony-Based Antileishmanial Compounds Prolong the Cardiac Action Potential by an Increase in Cardiac Calcium Currents. *Mol. Pharmacol.* **2006**, *69*, 1216–1225.
- (67) Ames, B. N.; McCann, J.; Yamasaki, E. Methods for Detecting Carcinogens and Mutagens with the *Salmonella*/Mammalian-Microsome Mutagenicity Test. *Mutat. Res. Mutagen. Relat. Subj.* **1975**, *31*, 347–363.
- (68) Basu, A. K. DNA Damage, Mutagenesis and Cancer. Int. J. Mol. Sci. 2018, 19, 970-982.
- (69) Hailu, G. S.; Robaa, D.; Forgione, M.; Sippl, W.; Rotili, D.; Mai, A. Lysine Deacetylase Inhibitors in Parasites: Past, Present, and Future Perspectives. J. Med. Chem. 2017, 60, 4780–4804.
- (70) Andrews, K. T.; Haque, A.; Jones, M. K. HDAC Inhibitors in Parasitic Diseases. *Immunol. Cell Biol.* **2012**, *90*, 66–77.
- (71) Kaur, S.; Shivange, A. V.; Roy, N. Structural Analysis of Trypanosomal Sirtuin: An Insight for Selective Drug Design. *Mol. Divers.* **2010**, *14*, 169–178.
- (72) Kadam, R. U.; Tavares, J.; M, K. V.; Cordeiro, A.; Ouaissi, A.; Roy, N. Structure Function Analysis of *Leishmania* Sirtuin: An Ensemble of In Silico and Biochemical Studies. *Chem. Biol. Drug Des.* **2008**, *71*, 501–506.
- (73) Zhang, Y. I-TASSER Server for Protein 3D Structure Prediction. BMC Bioinformatics 2008, 9, 40.
- (74) Ronin, C.; Costa, D. M.; Tavares, J.; Faria, J.; Ciesielski, F.; Ciapetti, P.; Smith, T. K.; MacDougall, J.; Cordeiro-da-Silva, A.; Pemberton, I. K. The Crystal Structure of the

- Leishmania infantum Silent Information Regulator 2 Related Protein 1: Implications to Protein Function and Drug Design. *PLoS One* **2018**, *13*, e0193602.
- (75) Vergnes, B.; Sereno, D.; Madjidian-Sereno, N.; Lemesre, J.-L.; Ouaissi, A. Cytoplasmic SIR2

 Homologue Overexpression Promotes Survival of *Leishmania* Parasites by Preventing

 Programmed Cell Death. *Gene* **2002**, *296*, 139–150.
- (76) Sixto-López, Y.; Gómez-Vidal, J. A.; Correa-Basurto, J. Exploring the Potential Binding Sites of Some Known HDAC Inhibitors on Some HDAC8 Conformers by Docking Studies. *Appl. Biochem. Biotechnol.* **2014**, *173*, 1907–1926.
- (77) Lawson, M.; Uciechowska, U.; Schemies, J.; Rumpf, T.; Jung, M.; Sippl, W. Inhibitors to Understand Molecular Mechanisms of NAD+-Dependent Deacetylases (Sirtuins). *Biochim. Biophys. Acta BBA Gene Regul. Mech.* **2010**, *1799*, 726–739.
- (78) Botta, C. B.; Cabri, W.; Cini, E.; De Cesare, L.; Fattorusso, C.; Giannini, G.; Persico, M.; Petrella, A.; Rondinelli, F.; Rodriquez, M.; Russo, A.; Taddei, M. Oxime Amides as a Novel Zinc Binding Group in Histone Deacetylase Inhibitors: Synthesis, Biological Activity, and Computational Evaluation. *J. Med. Chem.* **2011**, *54*, 2165–2182.
- (79) Turkevich, J.; Stevenson, P. C.; Hillier, J. A Study of the Nucleation and Growth Processes in the Synthesis of Colloidal Gold. *Discuss. Faraday Soc.* **1951**, *11*, 55–75.
- (80) Zauli-Nascimento, R. C.; Miguel, D. C.; Yokoyama-Yasunaka, J. K. U.; Pereira, L. I. A.; Pelli de Oliveira, M. A.; Ribeiro-Dias, F.; Dorta, M. L.; Uliana, S. R. B. In Vitro Sensitivity of Leishmania (Viannia) braziliensis and Leishmania (Leishmania) amazonensis Brazilian Isolates to Meglumine Antimoniate and Amphotericin B. Trop. Med. Int. Health 2010, 15, 68–76.
- (81) van der Meel, R.; Oliveira, S.; Altintas, I.; Haselberg, R.; van der Veeken, J.; Roovers, R. C.; van Bergen en Henegouwen, P. M. P.; Storm, G.; Hennink, W. E.; Schiffelers, R. M.; Koka, R. J. Tumor-Targeted Nanobullets: Anti-EGFR Nanobody-Liposomes Loaded with Anti-IGF-1R Kinase Inhibitor for Cancer Treatment. J. Controlled Release 2012, 159, 281–289.

- (82) Zamboni, D. S.; Rabinovitch, M. Nitric Oxide Partially Controls *Coxiella burnetii* Phase II Infection in Mouse Primary Macrophages. *Infect. Immun.* **2003**, *71*, 1225–1233.
- (83) Martin-Sanchez, J.; Lopez-Lopez, M. C.; Acedo-Sanchez, C.; Castro-Fajardo, J. J.; Pineda, J. A.; Morillas-Marquez, F. Diagnosis of Infections with *Leishmania infantum* Using PCR-ELISA. *Parasitology* 2001, 122, 607–615.
- (84) Corpas-López, V.; Merino-Espinosa, G.; Acedo-Sánchez, C.; Díaz-Sáez, V.; Morillas-Márquez, F.; Martín-Sánchez, J. Hair Parasite Load as a New Biomarker for Monitoring Treatment Response in Canine Leishmaniasis. *Vet. Parasitol.* **2016**, *223*, 20–25.
- (85) Luria, S. E.; Delbrück, M. Mutations of Bacteria from Virus Sensitivity to Virus Resistance. *Genetics* **1943**, *28*, 491–511.
- (86) Hubbard, S. A.; Green, M. H. L.; Gatehouse, D.; Bridges, J. W. The Fluctuation Test in Bacteria. In *Handbook of Mutagenicity Test Procedures (Second Edition)*; Kilbey, B. J., Legartor, M., Nichols, W., Ramel, C., Eds.; Elsevier: Amsterdam, 1984; pp 141–160.
- (87) Gilbert, R. I. The Analysis of Fluctuation Tests. *Mutat. Res. Mutagen. Relat. Subj.* **1980**, 74, 283–289.
- (88) Sixto-López, Y.; Bello, M.; Rodríguez-Fonseca, R. A.; Rosales-Hernández, M. C.; Martínez-Archundia, M.; Gómez-Vidal, J. A.; Correa-Basurto, J. Searching the Conformational Complexity and Binding Properties of HDAC6 through Docking and Molecular Dynamic Simulations. J. Biomol. Struct. Dyn. 2017, 35, 2794-2814.
- (89) Xu, D.; Zhang, Y. Improving the Physical Realism and Structural Accuracy of Protein Models by a Two-Step Atomic-Level Energy Minimization. *Biophys. J.* 2011, 101, 2525–2534.
- (90) Laskowski, R. A.; Rullmann, J. A. C.; MacArthur, M. W.; Kaptein, R.; Thornton, J. M. AQUA and PROCHECK-NMR: Programs for Checking the Quality of Protein Structures Solved by NMR. *J. Biomol. NMR* **1996**, *8*, 477–486.

- (91) Colovos, C.; Yeates, T. O. Verification of Protein Structures: Patterns of Nonbonded Atomic Interactions. *Protein Sci.* **1993**, *2*, 1511–1519.
- (92) Wiederstein, M.; Sippl, M. J. ProSA-Web: Interactive Web Service for the Recognition of Errors in Three-Dimensional Structures of Proteins. *Nucleic Acids Res.* **2007**, *35*, W407–W410.
- (93) Sippl, M. J. Recognition of Errors in Three-Dimensional Structures of Proteins. *Proteins Struct. Funct. Bioinforma.* **1993**, *17*, 355–362.
- (94) Trott, O.; Olson, A. J. AutoDock Vina: Improving the Speed and Accuracy of Docking with a New Scoring Function, Efficient Optimization, and Multithreading. *J. Comput. Chem.* 2009, 31, 455–461.
- (95) Morris, G. M.; Huey, R.; Lindstrom, W.; Sanner, M. F.; Belew, R. K.; Goodsell, D. S.; Olson, A. J. AutoDock4 and AutoDockTools4: Automated Docking with Selective Receptor Flexibility. J. Comput. Chem. 2009, 30, 2785–2791.
- (96) Gaussian O3, Revision C.O2, Frisch, M. J.; Trucks, G. W.; Schlegel, H. B.; Scuseria, G. E.; Robb, M. A.; Cheeseman, J. R.; Montgomery, Jr., J. A.; Vreven, T.; Kudin, K. N.; Burant, J. C.; Millam, J. M.; Iyengar, S. S.; Tomasi, J.; Barone, V.; Mennucci, B.; Cossi, M.; Scalmani, G.; Rega, N.; Petersson, G. A.; Nakatsuji, H.; Hada, M.; Ehara, M.; Toyota, K.; Fukuda, R.; Hasegawa, J.; Ishida, M.; Nakajima, T.; Honda, Y.; Kitao, O.; Nakai, H.; Klene, M.; Li, X.; Knox, J. E.; Hratchian, H. P.; Cross, J. B.; Bakken, V.; Adamo, C.; Jaramillo, J.; Gomperts, R.; Stratmann, R. E.; Yazyev, O.; Austin, A. J.; Cammi, R.; Pomelli, C.; Ochterski, J. W.; Ayala, P. Y.; Morokuma, K.; Voth, G. A.; Salvador, P.; Dannenberg, J. J.; Zakrzewski, V. G.; Dapprich, S.; Daniels, A. D.; Strain, M. C.; Farkas, O.; Malick, D. K.; Rabuck, A. D.; Raghavachari, K.; Foresman, J. B.; Ortiz, J. V.; Cui, Q.; Baboul, A. G.; Clifford, S.; Cioslowski, J.; Stefanov, B. B.; Liu, G.; Liashenko, A.; Piskorz, P.; Komaromi, I.; Martin, R. L.; Fox, D. J.; Keith, T.; Al-Laham, M. A.; Peng, C. Y.; Nanayakkara, A.; Challacombe, M.;

- Gill, P. M. W.; Johnson, B.; Chen, W.; Wong, M. W.; Gonzalez, C.; and Pople, J. A.; Gaussian, Inc., Wallingford CT, 2004.
- (97) Gaussian 09, Revision A.02, M. J. Frisch, G. W. Trucks, H. B. Schlegel, G. E. Scuseria, M. A. Robb, J. R. Cheeseman, G. Scalmani, V. Barone, G. A. Petersson, H. Nakatsuji, X. Li, M. Caricato, A. Marenich, J. Bloino, B. G. Janesko, R. Gomperts, B. Mennucci, H. P. Hratchian, J. V. Ortiz, A. F. Izmaylov, J. L. Sonnenberg, D. Williams-Young, F. Ding, F. Lipparini, F. Egidi, J. Goings, B. Peng, A. Petrone, T. Henderson, D. Ranasinghe, V. G. Zakrzewski, J. Gao, N. Rega, G. Zheng, W. Liang, M. Hada, M. Ehara, K. Toyota, R. Fukuda, J. Hasegawa, M. Ishida, T. Nakajima, Y. Honda, O. Kitao, H. Nakai, T. Vreven, K. Throssell, J. A. Montgomery, Jr., J. E. Peralta, F. Ogliaro, M. Bearpark, J. J. Heyd, E. Brothers, K. N. Kudin, V. N. Staroverov, T. Keith, R. Kobayashi, J. Normand, K. Raghavachari, A. Rendell, J. C. Burant, S. S. Iyengar, J. Tomasi, M. Cossi, J. M. Millam, M. Klene, C. Adamo, R. Cammi, J. W. Ochterski, R. L. Martin, K. Morokuma, O. Farkas, J. B. Foresman, and D. J. Fox, Gaussian, Inc., Wallingford CT, 2016.
- (98) Varetto, U. Molekel 5.4.0.8, Swiss National Supercomputing Centre, Manno (Switzerland). Molekel.
- (99) Gasteiger, J.; Marsili, M. Iterative Partial Equalization of Orbital Electronegativity—a Rapid Access to Atomic Charges. *Tetrahedron* **1980**, *36*, 3219–3228.
- (100) Pettersen, E. F.; Goddard, T. D.; Huang, C. C.; Couch, G. S.; Greenblatt, D. M.; Meng, E. C.; Ferrin, T. E. UCSF Chimera—A Visualization System for Exploratory Research and Analysis. *J. Comput. Chem.* **2004**, *25*, 1605–1612.
- (101) The PyMOL Molecular Graphics System, Version 2.0 Schrödinger, LCC.

Table of contents

In vitro antileishmanial activity of compound **5** against viscerotropic and dermotropic *Leishmania* species (intracellular amastigotes):

Leishmania	IC ₅₀ (μM)
L. infantum	3.21 ± 1.2
L. donovani	2.91 ± 0.2
L. major	1.00 ± 0.3
L. tropica	0.71 ± 0.2

In vivo activity of compound **5** supported on gold nanoparticles against *Leishmania infantum*:

	Drug alone	Drug in combination
Target organ	(25 mg/Kg)	(meglumine antimoniate)
Spleen of BALB/c mice	96% reduction	92% reduction
Liver of BALB/c mice	68% reduction	100% reduction